İSTANBUL TECHNICAL UNIVERSITY ★ INSTITUTE OF SCIENCE AND TECHNOLOGY

NUMERICAL NOISE PREDICTION: APPLICATION TO RADIAL FANS

M.Sc. Thesis by
Yılmaz DOĞAN, Mechanical Eng.

Department : **Mechanical Engineering**

Programme: **Machine Dynamics, Vibration & Acoustics**

MAY 2007

İSTANBUL TECHNICAL UNIVERSITY ★ INSTITUTE OF SCIENCE AND TECHNOLOGY

NUMERICAL NOISE PREDICTION: APPLICATION TO RADIAL FANS

M.Sc. Thesis by
Yılmaz DOĞAN, Mechanical Eng.

(503041409)

Date of submission : 7 May 2007

Date of defence examination: 28 May 2007

Supervisor (Chairman): Prof. Dr. Kenan Y. ŞANLITÜRK

Members of the Examining Committee Prof.Dr. H. Temel BLEK

Prof.Dr. A. Rüstem ASLAN

MAY 2007

İSTANBUL TEKNİK ÜNİVERSİTESİ ★ FEN BİLİMLERİ ENSTİTÜSÜ

SAYISAL GÜRÜLTÜ MODELLEMESİ: RADYAL FAN UYGULAMASI

YÜKSEK LİSANS TEZİ

Makine Müh., Yılmaz DOĞAN
(503041409)

Tezin Enstitüye Verildiği Tarih : 7 Mayıs 2007
Tezin Savunulduğu Tarih : 28 Mayıs 2007

Tez Danışmanı :	**Prof.Dr. Kenan Y. ŞANLITÜRK**
Diğer Jüri Üyeleri	**Prof.Dr. H. Temel BELEK**
	Prof.Dr. A. Rüstem ASLAN

MAYIS 2007

ACKNOWLEDGMENTS

I would like to express my deepest gratitude to my advisor, Professor Kenan Yüce ŞANLITÜRK, for giving me the opportunity to work on this project and for his support, guidance and suggestions. It is a pleasure and honor being his student.

This study was carried out at the Department of R&D, Vibration & Acoustic Technologies Group. I wish to thank all the member of the R&D, in particular the people of Vibration & Acoustics for making this study a memorable one.

My deepest gratitude to Dr. Faruk BAYRAKTAR, for guiding me during this study, for lending his time, interest and insight.

Specifically I wish to thank Mr. Metin GÜL and Mr. Kenan ATAÇ for their help, for providing the experimental data and for making a nice atmosphere at the work.

Among the several contributions made to this thesis and the author himself, both personal and scientific, I wish to distinguish those made by Assoc. Prof. Dr. Esra SORGÜVEN and Mr. Ergin ARSLAN. The present work has benefited tremendously by their experiences and I would always remain indebted, as they have been kind mentors.

Finally, it's my deepest pride to thank here my mother and father. My journey has been their journey and this thesis is dedicated to their love.

May 2007 Yılmaz DOĞAN

TABLE OF CONTENTS

LIST OF TABLES

LIST OF FIGURES

NOMENCLATURE

c_v	specific heat at constant volume	
c_p	specific heat at constant pressure	
E	internal energy	[m^3/s^2]
ε_v	dissipation term	[m2/s3]
f_e	external forces	
h	static enthalpy	[J/kg]
H	enthalpy	[J/kg]
$\overline{\overline{I}}$	identity matrix	
κ	thermal conductivity	
p	pressure	[Pa]
q_H	contribution of heat sources	
T	temperature	[K]
ρ	density	[kg/m^3]
$\overline{\overline{\tau}}$	stress tensor	
$\vec{v}$	velocity vector	[m/s]
W_f	work done by external forces	
μ	absolute viscosity	[kg/(m.s)]
δ_{ij}	delta function	
ϕ	arbitrary flow variable	
$\overline{\phi}$	time average	
ϕ'	fluctuations	
$\widetilde{\phi}$	filtration	
Re	Reynold's number	
L	length-scale,	[m]
U	velocity-scale	[m/s}
υ	kinematic viscosity	[m2/s]
ℓ	integral length-scale	[m]

λ	Taylor length-scale	[m]
η	Kolmogorov length-scale	[m]
Re_T	turbulent Reynolds number	
k	specific turbulent kinetic energy	[m2/s2]
k	wave number	[1/m]
δ	boundary layer thickness	[m]
τ_{ij}	subgrig scale stress	[kg/(m.s2)]
T_{ij}	Lighthill stress tensor	[kg/(m.s2)]
R_{gas}	gas constant	[J/(kg.K)]
$\overline{\sigma_{ij}}$	viscous stress tensor,	[kg/(m.s2)]
A	amplitude of sound wave	[Pa]
c	speed of sound	[m/s]
f	frequency	[Hz]
f	aerodynamic force on a surface	[N/m2]
λ	wave length	[m]
ω	angular frequency	[Hz]
M	Mach number	
M_r	magnitude of the Mach vector $\vec{M}$ in the direction r	
y^+	dimensionless wall distance	
I	sound intensity	[Watt/m2]
SPL	sound pressure level	[dB]
t	time	[s]
u, v, w	streamvise, transverse, spanwise convection velocity	[m/s]
Δ	step size	
$APEs$	acoustic perturbation equations	
BC	boundary conditions	
CAA	computational aero acoustics	
DNS	direct numerical simulations	
FWH	Ffowcs Williams-Hawking	

LEE	linearized Euler equations	
LES	Large eddy simulations	
RANS	Reynolds Averaged Navier-Stokes	
D	diameter,	[m]
L_{ij}	Leonard stress,	[kg/(m.s^2)]
N_{pts}	number of grid points	
N_{ts}	number of time steps	
r	radius, [m]	
BEM	Boundary Element Method	
CAD	Computer Aided Drawing	
MRF	Multiple Reference Frame	
DBEM	Direct Boundary Element Method	
FEM	Finite Element Method	
FFT	Fast Fourier Transform	
CFD	Computational Fluid Dynamics	
IBEM	Indirect Boundary Element Method	
SM	Sliding Mesh	
MDBEM	Multi-Domain Direct Boundary Element Method	
SGS	Sub Grid Scale	

NUMERICAL NOISE PREDICTON: APPLICATION TO RADIAL FANS

SUMMARY

Predicting the flow-induced noise of a laundry dryer is essential in order to control the noise emission and to comply with the noise regulations and consumer demands. Experimental aero acoustics methods involve drawbacks due to time and investment expenses and measurement errors including reflection problems. With the improvement in computational technology, Computational Aero Acoustics (CAA) provides a proper model for noise generation and propagation. Especially, the hybrid CAA methods are efficient and inexpensive, since these solve for the different scales of noise generation and propagation separately.

In this thesis a hybrid CAA model is employed to predict the far field noise generated by a radial fan used in laundry dryers and based on the insight gained from the CAA analysis a new silent fan prototype is developed. Aero Acoustic computation of both fans is performed in two steps: i) computing the unsteady flow field and ii) computing the acoustic pressure fluctuations in the far field in the frequency domain. Flow field is solved with Large Eddy Simulation (LES), where the large and energetic scales of turbulence are resolved and the small and dissipative scales are modeled. Acoustic sources are computed based on the turbulent unsteady flow field, with the Ffowcs Williams and Hawkings equation. Finally, the wave equation is solved to determine the far field sound pressure level. The numerical results of the turbulent unsteady flow and noise emission are in good agreement with the experiments. This study shows how the CAA methods provide an insight to the turbulent flow and noise generation mechanisms and how these can be employed to decrease the overall sound pressure level of a fan.

SAYISAL GÜRÜLTÜ MODELLEMESİ: RADYAL FAN UYGULAMASI

ÖZET

Müşteri beklentileri ve gürültü denetim politikaları göz önüne alındığında kurutucu fanlarına ait gürültü kestirimi nem kazanmaktadır. Deneysel çalışmalar, büyük maliyetler getirmekte ve önemli cihaz ve insan kaynağına gerek duymaktadır. Bilgisayar teknolojisinin gelişmesiyle birlikte, Hesaplamalı Aero Akustik (HAA) gürültü oluşum ve yayınımına yönelik kullanılabilir bir yöntem ortaya koymaktadır. Özellikle hibrid HAA, gürültünün oluşumu ve yayınımı hesaplamalarını birbirinden ayrı çözümlediği için, pahalı olmayan ve etkili bir yaklaşım ortaya koymaktadır.

Bu çalışmada, çamaşır kurutucularında kullanılan radyal fan uzak alan gürültüsünün kestirimi için hibrih HAA yöntemi ortaya konmaktadır. Radyal fanlara yönelik HAA özümleme iki aşamadan oluşmaktadır: i) akış alanının çözümlenmesi ve ii) uzak alan ses yayınımının hesaplanması. Akış alanı Büyük Girdap Simülasyonu (LES) türbülans modellemesi kullanılarak çözümlenmiştir. LES akışa ait büyük girdapları çözen, küçük girdapları ise modelleyen bir yöntem olduğundan, HAA için mevcut bilgisayar teknolojisi göz önüne alındığında en uygun çözümdür. Türbülatif akış alanı çözümlemesinden sonra, fan kanatları ve salyangoz üzerindeki basın titreşimleri hesaplanarak akustik kaynaklar (dipoller) hesaplanmış ve Ffowcs Williams ve Hawkings ve dalga denklemleri kullanılarak uzak alan ses yayınımı hesaplanmıştır. Sayısal sonuçlar deneysel sonuçlar ile karşılaştırılmıştır. Oluşturulan metodoloji ile elde edilen sonuçlar deneysel sonuçlar ile oldukça iyi bir uyum göstermekte olup, ses basıncı yanında sesin yönelimi de hesaplanmıştır.

1. INTRODUCTION

1.1. Motivation

Noise reduction is among the most important design criteria in a variety of technical fields and a challenging task in mechanical engineering. The increasing awareness on the effects of noise on physiological and psychological health and the resulting strict governmental regulations concerning the noise emission, enforce designers to focus on noise reduction more than ever. Especially the recent governmental regulations enforce noise reduction in aerospace engineering, climatization and fluid machinery. An adequate noise prediction is necessary in order to reduce noise emission satisfactorily and to prevent expensive after-design treatments. The goal of this study is to build a reliable and efficient tool to predict the far field noise of fluid machinery. Primary application area of this tool will be industrial problems. Therefore, the noise prediction tool has to fulfill certain requirements. First of all, it has to provide a detailed insight of the noise generation mechanisms. A prerequisite of noise reduction is the knowledge on the characteristics of noise generation. Based on this knowledge, main noise sources can be determined and eliminated. Furthermore, the tool has to be precise and economical in terms of the human and computing resources.

Empirical or semi-empirical methods of noise reduction do not suffice for this purpose, since they fail to provide detailed information. Experiments are very time consuming and too costly in terms of financial and human resources. Furthermore they are time-consuming. Semi-empirical or analytical methods are usually boxed on numerous assumptions and fail to provide insight and involve numerous assumptions. Therefore, computational methods of noise prediction are valuable alternatives to these methods.

1.2. Literature

Studies involving analysis, prediction and reduction of fan noise are active research areas because of the widespread use of axial and centrifugal fans in industry.

Sir James Lighthill [1, 2, 3] published three articles which provide the theory of aerodynamic noise generation for describing the radiation of the sound field generated by turbulent flow. In his “acoustic analogy”, he derived an inhomogeneous wave equation with the presence of the acoustic sources derived from compressible equations for fluid motion. Curle [4] contributed the effect of solid surfaces on sound generation and by Ffowcs Williams and Hawkings [5] the effect of moving solid surfaces on sound generation contributed to the acoustic analogy.

The simplest approach for computing the flow field is based on a numerical solution of the Reynolds Averaged Navier-Stokes equations (RANS) with appropriate turbulence model. Page et. al. [6] have coupled the standard RANS ($k-\varepsilon$) with the Lighthill acoustic analogy for studying coaxial jet noise. Bailly et. al. [7] obtained the aerodynamic field from a numerical solution of RANS associated with a $k-\varepsilon$ closure. The major drawback with RANS is due to the large error in estimating the acoustic sources. Since only information about the local mean flow is used in RANS, solutions based on RANS cannot predict the unsteadiness of the flow field and hence the dynamics of the acoustic sources.

More realistic approaches are using Large Eddy Simulation (LES) or Direct Numerical Simulation (DNS) which can capture the dynamics of turbulence. Using LES, Bogey et. al. [8] investigated a subsonic circular jet with a Mach number of 0.9 and Reynolds number of 65000. The acoustic field and the acoustic sources were investigated from the perspective of the dilatation (divergence of velocity). This accounts only for compressible fluctuations and is linked to the acoustic pressure outside the jet. In concordance with the experimental observations, predominant sound sources were found just after the end of the potential core region. This shows the feasibility of the direct computation of the sound generated by turbulence using LES. Ewert et. al. [9] applied a hybrid method based on LES of compressible flow and Acoustic Perturbation Equations (APEs) to predict the trailing edge noise.

Fan noise involves both tonal and broad band components: Tonal noise due to blade passing and broad band due to turbulent fluctuations and the interaction with casing resonance caused by the excitation of a natural acoustic frequency.

Numerical fan noise prediction usually investigates tonal and broadband noise separately. The studies of Gutin are considered as the pioneer work about the acoustics of axial flow machinery, which were published in the late 40's [10]. Recently, Carolus [12] and Bommes et. al. [11] have made notable contributions about the aerodynamics and the acoustics of the fans.

Velarde et. al. [13] implemented a predictive maintenance methodology and applied to a squirrel-cage fan. The experimental investigation involved acoustic pressure and acceleration measurements in different locations for different operating conditions and followed by a simple analysis in which the spectra of acoustic pressure and acceleration signals in different conditions are compared. This study shows that the selected signals can be enough to detect failures in the selected fan.

Marretta et. al. [14] implemented $k-\varepsilon$ method for obtaining the unsteady characteristics of a realistic turbulent flow interacting with a rectangular flat plate undergoing ''ground effect''. The far-field acoustic calculation is facilitated by the Kambe model (from Lighthill's theory) and an original post-processor has been developed to determine the far-field spectra and the source term characteristics.

Ianniello [15] studied and obtained noise generated by a high tip-speed rotating blade in time domain through the Ffowcs Williams–Hawkings (FW-H) equation and a numerical procedure developed to model the so called 'emission surface'. He accounted for the contribution of the supersonic sources and while reducing the computational effort and to treat some advanced (rotor and propeller) configurations. The method is tested on some complex blade geometries and proved to be robust and effective in predicting both the FW-H linear terms from a supersonic tip speed blade and the quadrupole source terms for a hovering rotor at delocalized operating condition.

Lin et. al. [16] designed a small Forward–Curved (FC) centrifugal fan under the space limitations of notebook computers with the emphasis on the blade shape, blade inlet angle and the outlet geometry of the housing. The flow patterns throughout the fan are visualized using numerical techniques. A good agreement between the experimental and numerical results indicates a great potential to reduce expensive experimental work by using Computational Fluid Dynamics (CFD) tools.

Jeon et. al. [17] developed a method to calculate the unsteady flow fields and Aero Acoustic sound pressure in the centrifugal fan of a vacuum cleaner. Unsteady flow-field data are calculated by the vortex method. The sound pressure is then calculated by an acoustic analogy. The predicted tonal sound pressure levels spectra of an acoustic pressure agree very well with the measured data within 4dBA deviation range.

Suh et. al. [18] developed a LES code and tested for both attached and separated wall-bounded turbulent flows. The code combines the low-dissipation and dispersion through the use of a sixth-order accurate, compact finite-difference scheme for spatial derivatives. LES predictions were in reasonable agreement with previous numerical and experimental data for fully developed turbulent channel flow and turbulent separated flow in a planar asymmetric diffuser.

Bogey et. al. [19] investigated both the flow and the sound fields of an isothermal jet by large eddy simulation (LES) on two grids. They found the mean flow and turbulence properties, as well as the sound pressure field, compare favorably with experimental data on similar jets.

Ryu et. al.[20] studied the unsteady flow field from the quick-opening throttle valve by applying compressible CFD techniques and its corresponding frequency-domain acoustic pressure was predicted by using the integral formula derived from the wave equation with the modeled source term by using the General Green Function. They claimed that the predicted acoustic pressure levels show reasonable agreement with the measured data.

Nallasamy et. al. [21] studied the rotor wake turbulence stator interaction broadband noise. The computations employ the wake flow turbulence information from computational fluid dynamic solutions. It is claimed that the predicted acoustic power levels and shape of the spectra show reasonable agreement with the measured spectra for the exhaust noise at approach condition.

Kim et. al. [22] studied the flow mechanism of discrete frequency noise from a symmetrical airfoil in a uniform flow by the numerical simulation. It is showed that the turbulent boundary layer is formed over the suction side of the airfoil and the quasi-periodic behavior of negative vortex formation on the suction side is affected by the strength and the periodicity of positive vortices near the trailing edge. A hybrid method using acoustic analogy of Curle's formula of a free-space acoustic Green's function was employed to compute the far-field sound spectrum

Gérard et. al. [23] developed an inverse Aero Acoustic model aiming at reconstructing the aerodynamic forces (dipole strength distribution) acting by the fan blades at multiples of the Blade Passing Frequency (BPF) on the fluid that relates the unsteady forces to the radiated sound field. Numerical simulations and experimental results are done for to reconstruct the dipole strength distribution over the fan surface.

Maaloum et. al. [24] studied experimentally the presence of the duct contour and lack influence on the acoustic signature of a fan.

Velarde et. al. [25] studied the experimental determination of the tonal noise sources in a centrifugal fan. This study shows that, a strong source of noise caused by the interaction between the fluctuating flow leaving the impeller and the volute tongue is appreciable. And also, the unsteady forces exerted on the fan blades constitute another noise generation mechanism, which affects the whole extension of the impeller, thus transmitting pressure fluctuations to the entire volute casing.

Polacsek et. al. [26] applied noise control technique to reduce rotor–stator interaction noise of subsonic fans. In addition, the system has been investigated numerically via 2- unsteady Reynolds averaged Navier–Stokes solver, providing the unsteady blade and vane forces required as inputs for acoustics, has been coupled to a BEM code (SYSNOISE), solving the Helmholtz equation. Interaction noise sources are expressed by the Ffowcs- Williams and Hawkings equation. Interaction mode levels predicted by the computations are within 1.5 dB of experiment.

Özyörük et. al. [27] developed a frequency-domain method for predicting sound fields of ducted fans based on the solution of the frequency-domain form of the Euler equations linearized about an axisymmetric non-uniform background flow. By comparing the simulations of the former geometry to the available experimental data, it is claimed that the developed method can predict the forward arc far-field sound of turbofans, including the attenuation effects of liners.

Wu et. al. [28] developed a semi-empirical formula capable of simulating both narrow and broad band sounds of the spectra for the tested axial flow fans in a free-field.

Wu et. al. [29] also developed a computer model for estimating the noise performance of an engine cooling fan assembly. The computer model thus obtained is validated experimentally on five sets of completely different engine cooling fan assemblies. It is claimed that the calculated noise spectra compare well with measured data.

Kato et. al. [30] numerically predicted the sound generated from flows with a low Mach number based on Lighthill's Acoustic Analogy. The source fluctuations of the flow field are computed with a large-eddy simulation (LES) of incompressible fluid with Dynamic Smagorinsky Model (DSM) and they are fed to the following acoustical computation as input data. The far-field sound generated from flow around a rear-view mirror for use in automobiles is computed based on Lighthill–Curle's equation by using the surface pressure fluctuations computed by the LES. Then, the internal flow of a multi-stage centrifugal pump and radiated sound are simulated where blade-stator interaction is the primary source of sound generation. Finally, the sound due to a transitional boundary layer on an aerofoil is computed for which the scattering effects of high-frequency sound at a non-compact body is taken into account by solving the wave equation in the frequency domain.

Velarde et. al. [31] studied a three-dimensional numerical simulation of the complete unsteady flow on the whole impeller-volute configuration of a centrifugal fan. It is claimed that, numerical results have been contrasted using experimental investigations, showing a good agreement.

Lee et. al. [32] investigated the rotor high speed impulsive noise with a combined CFD-Kirchhoff method and the results are compared with experimental data for a hovering rotor at high hover Mach numbers.

Liow et. al. [33] presented a numerical investigation into the acoustic radiation from laminar flow past a two-dimensional rectangular cylinder. A two-step Aero Acoustic prediction method was used where the incompressible flow equations were first solved numerically followed by computation of the time-evolving acoustic field by solving the acoustic wave equation directly.

2. THEORY AND PRINCIPLES OF FLOW ACOUSTICS

Acoustics is the science of sound that includes its production, propagation and its effects. The acoustic theory is derived from fluid mechanics and focuses on the mathematical description of sound waves. [33]

Computational Aero Acoustics (CAA) is used to investigate the noise generation and propagation mechanisms with the help of fluid dynamics and mathematical description of the sound waves. The main computational approaches evaluate the sound field directly from turbulent flow data and provide an insight to the relation between the aerodynamics of the flow and related sound emission.

Modern CAA techniques can be separated into two steps; the first step is the determination of the unsteady flow data and the second step is the computation of the acoustic signal [10]. Unsteady flow field can be predicted by computational methods which eliminate the disadvantages of experiments such as limited temporal and spatial resolutions and huge cost of the experimental test facilities. Recent developments in computational technology enabled flow simulation methodologies may be used to study the problems related to sound generation with high accuracy within reasonable CPU-times.

Aero Acoustic computation in noise prediction is performed in two steps: computing the unsteady flow field and computing the density and pressure fluctuations in frequency or time domain. At low mach numbers, the main difficulty in the calculation of sound generated by fluid flow is the occurrence of different scales [34]. Radiated sound waves have a long wavelength with small amount of energy. On the other hand, fluid flow dominated by small spatial structures with large amount of energy, such as small vortices in a turbulent flow.

Direct computation of sound field with DNS and LES can calculate both the unsteady flow field and the acoustic signal associated with it. For direct computation of sound field the domain on which the problem is solved must include the noise-production region and at least a part of the acoustic near-field [33]. DNS model, since it solves the Navier-Stokes equation without any modeling approximations and aims to resolve the whole range of time and length scales; from integral scales to Kolmogorov scales and LES methods, which resolves the large and energetic scales of turbulence and models the small and dissipative scales can be used to calculate both the unsteady flow field and the acoustic signal associated with it. The main disadvantage of such methods is the enormous computational cost of such direct calculations, this being the main reason for which only relatively simple flow configurations at modest Reynolds numbers were studied [33].

To save computational time and add the effects of the structures, hybrid approaches can be used. . In contrast with the direct methods the hybrid methods comprise two parts. First, the unsteady flow field is computed. The unsteady flow field can be computed using the unsteady Reynolds Averaged Navier-Stokes equations, Large Eddy Simulation or Direct Numerical Simulation. Available CPU capacity and flow characteristics (like Re, Ma, etc.) are main constraints for the choice of the simulation model. Then, in the second step, acoustic sources are computed.

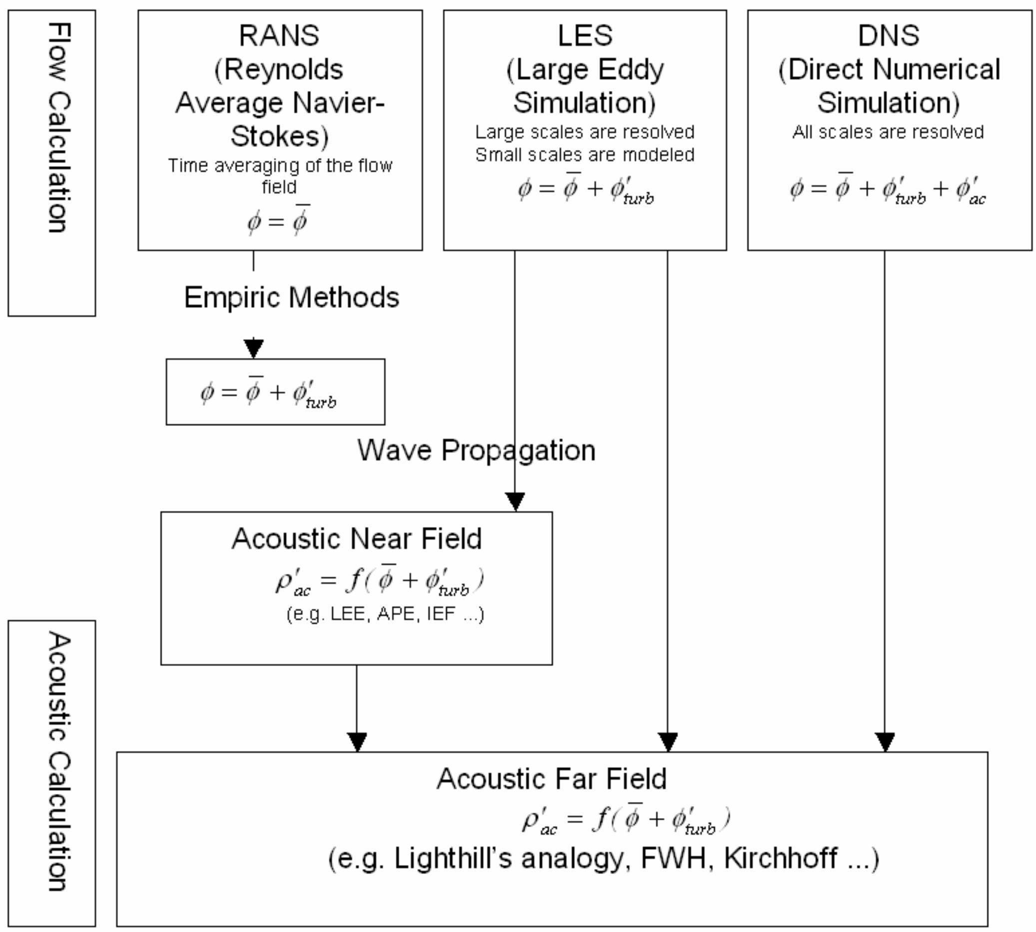

Figure 2.1: Overview of the modern CAA methods

In Figure 2.1, an overview of the modern CAA methods is given. As seen in figure above, Modern CAA techniques can be separated into two steps; the first step is the determination of the unsteady flow data (flow calculation) and the second step is the computation of the acoustic signal (acoustic calculation). Flow calculation part includes the calculation of flow parameters using the unsteady Reynolds Averaged Navier-Stokes equations (uRANS), Large Eddy Simulation (LES) or Direct Numerical Simulation (DNS). Flow parameters can be divided as follows: $\overline{\phi}$ is the mean value, ϕ'_{turb} is the turbulent value and ϕ'_{ac} is the acoustic value of the flow parameters. With DNS, one can solve all the scales and obtain the mean, turbulent and acoustic values of the flow parameters.

2.1. Theory of Computational Fluid Dynamics

2.1.1. Governing equations

For Aero Acoustic computation, boundary layer has to be resolved with high accuracy to determine the pressure fluctuations over the surface of a fan blade. Navier-Stokes equations are adequate to describe the time-dependent behavior of three regimes, namely laminar, transitional and turbulent generally noticed in a flow field. The Navier-Stokes equations consist of three fundamental equations: conservation of mass, conservation of momentum and conservation of energy. They are expressed in a conservative form in a Cartesian coordinate system as:

$$\frac{\partial}{\partial t}\begin{pmatrix}\rho \\ \rho\vec{v} \\ \rho E\end{pmatrix} + \vec{\nabla}\cdot\begin{pmatrix}\rho\vec{v} \\ \rho\vec{v}\otimes\vec{v} + p\overline{\overline{I}} - \overline{\overline{\tau}} \\ \rho\vec{v}H - \overline{\overline{\tau}}\cdot\vec{v} - \kappa\nabla T\end{pmatrix} = \begin{pmatrix}0 \\ \rho\vec{f}_e \\ W_f + q_H\end{pmatrix} \tag{1}$$

where ρ is the density, $\vec{v}$ is the velocity vector, E is the internal energy, H is the enthalpy, p is the pressure, $\overline{\overline{\tau}}$ is the stress tensor, $\overline{\overline{I}}$ is the identity matrix, κ is the thermal conductivity of the fluid and q_H represents the contribution of heat sources. f_e represents external forces, with W_f being the work done by external forces, $W_f = \rho\vec{f}_e\cdot\vec{v}$. The coefficients of the stress tensor, $\overline{\overline{\tau}}$ for Newtonian fluids are given by

$$\tau_{ij} = \mu(T,p)\left[\left(\partial_i v_j + \partial_j v_i\right) - \frac{2}{3}\left(\vec{\nabla}\cdot\vec{v}\right)\delta_{ij}\right] \tag{2}$$

where μ is the absolute viscosity of the fluid and δ_{ij} is the delta function which is one on the diagonal and is zero elsewhere.

Assuming the sources are known, we have unknown thermodynamic variables ρ, u, v, w, T, p, s and h or e. h and e are functions of two of the other variables (p and T). This can be shown by rewriting the energy equation as an equation for internal energy

$$\rho\frac{\partial e}{\partial t} = -p(\vec{\nabla}\cdot\vec{v}) + \vec{\nabla}\cdot(\kappa\nabla T) + \varepsilon_v + q_H \tag{3}$$

or static enthalpy (h)

$$\rho\frac{\partial h}{\partial t} = \frac{dp}{dt} + \vec{\nabla}\cdot(\kappa\nabla T) + \varepsilon_v + q_H \tag{4}$$

where ε_v is the dissipation term,

$$\varepsilon_v = \left(\overline{\overline{\tau}}\cdot\nabla\right)\cdot\vec{v} \tag{5}$$

We can then remove e and h from the energy equation by applying one of the relationships

$$de = c_v dT \text{ or } dh = c_p dT \tag{6}$$

to Eqs. (3) or (4). c_v and c_p are the specific heats of the fluid at constant volume and pressure, respectively. By assuming a perfect gas, we gain an additional equation, the equation of state:

$$p = \rho RT \tag{7}$$

We now have six equations and six unknowns. The entropy is de-coupled and can be found independently of the flow solution from basic thermodynamics:

$$Tds = dh - \frac{dp}{\rho} \tag{8}$$

2.1.2. Turbulence and its modeling

Three different regimes, namely laminar, transitional and turbulent, can generally be noticed in a flow field [35]. In turbulent flows, the time-averaged flow parameters fluctuate in all three spatial dimensions. Due to the instability of the laminar state, flow changes from laminar to turbulent, with the amplified small disturbances. After the rotational flow structures are developed, the turbulent kinetic energy is transferred from larger eddies to smaller ones, with the smallest eddies eventually dissipating into heat through molecular viscosity.

The choice of the turbulence model is directly related to the goals of the simulation. Flow induced noise prediction aims to compute the acoustic signal of technically relevant flows; either uRANS or LES was chosen as the turbulence model.

A non-dimensional parameter for flow behavior is the Reynolds number:

$$\mathrm{Re} = \frac{UL}{\nu} \tag{9}$$

where U and L are characteristic velocity and length scales of the mean flow and ν is the kinematic viscosity of the fluid. According to Reynolds number, turbulence occurs when the convection is much stronger than the dissipation.

A turbulent flow field at high Reynolds number consists of vortices (eddies) of various sizes, from the largest to the smallest ones. Each eddy can be related to a scale of velocity, time and length. These initial large vortical scales will brake up due to vortex stretching to develop smaller and smaller scale structures [35].

Three different length scales are often referred to a turbulent flow field: i) the integral length scale (l), ii) the Taylor microscale (λ) and iii) the Kolmogorov microscale (η).

The largest scales of turbulence can be estimated by the integral length scale. This represents the mean distance for which the velocity fluctuations are correlated. The integral scales, often referred to as energy-bearing eddies, is related to ε, so that

$$\eta / \ell \sim \mathrm{Re}_T^{-3/4}$$

where $Re_T = k^{1/2}\ell / \upsilon$ is the usual turbulence Reynolds number. Since values of Re_T greater of 10^4 are typical of fully developed turbulent boundary layers and $\ell \sim 0.1\delta$ where δ is boundary-layer thickness.

For isotropic turbulence, Taylor microscale is defined by

$$\varepsilon = 15\upsilon\overline{\left(\frac{\partial u'}{\partial x}\right)^2} \equiv 15\upsilon\frac{\overline{u'^2}}{\lambda^2} \tag{10}$$

The smallest scales in turbulence are the Kolmogorov scales. Kolmogorov scales of length, time and velocity are

$$\eta \equiv \left(\upsilon^3 / \varepsilon\right)^{1/4} \quad \tau \equiv \left(\upsilon / \varepsilon\right)^{1/2} \quad \upsilon \equiv \left(\upsilon\varepsilon\right)^{1/4} \tag{11}$$

Kolmogorov length scale, (η) outside the viscous wall region is less than 1/1000 times the thickness of the boundary layer [36].

As shown in Fig. 2.2 three distinct regions of turbulent eddies can be identified, namely the energy containing eddies, the inertial subrange and the dissipation subrange. The integral scale, which is determined by the geometry of the flow, contains most of the turbulent kinetic energy. This energy is continuously supplied by the mean flow. The Taylor microscale is in the inertial sub range and is much smaller than the integral scale but it is much larger than the Kolmogorov microscale. Turbulence scales that are part of the inertial subrange receive energy from the larger scales of turbulence and subsequently they loose energy by transferring it to the smaller scales. This process is named "the energy cascade". The smallest length scales (Kolmogorov) in the energy spectrum are in the dissipation subrange. At this level the viscosity is important and the entire kinetic energy of eddies is transferred into heat by viscous dissipation.

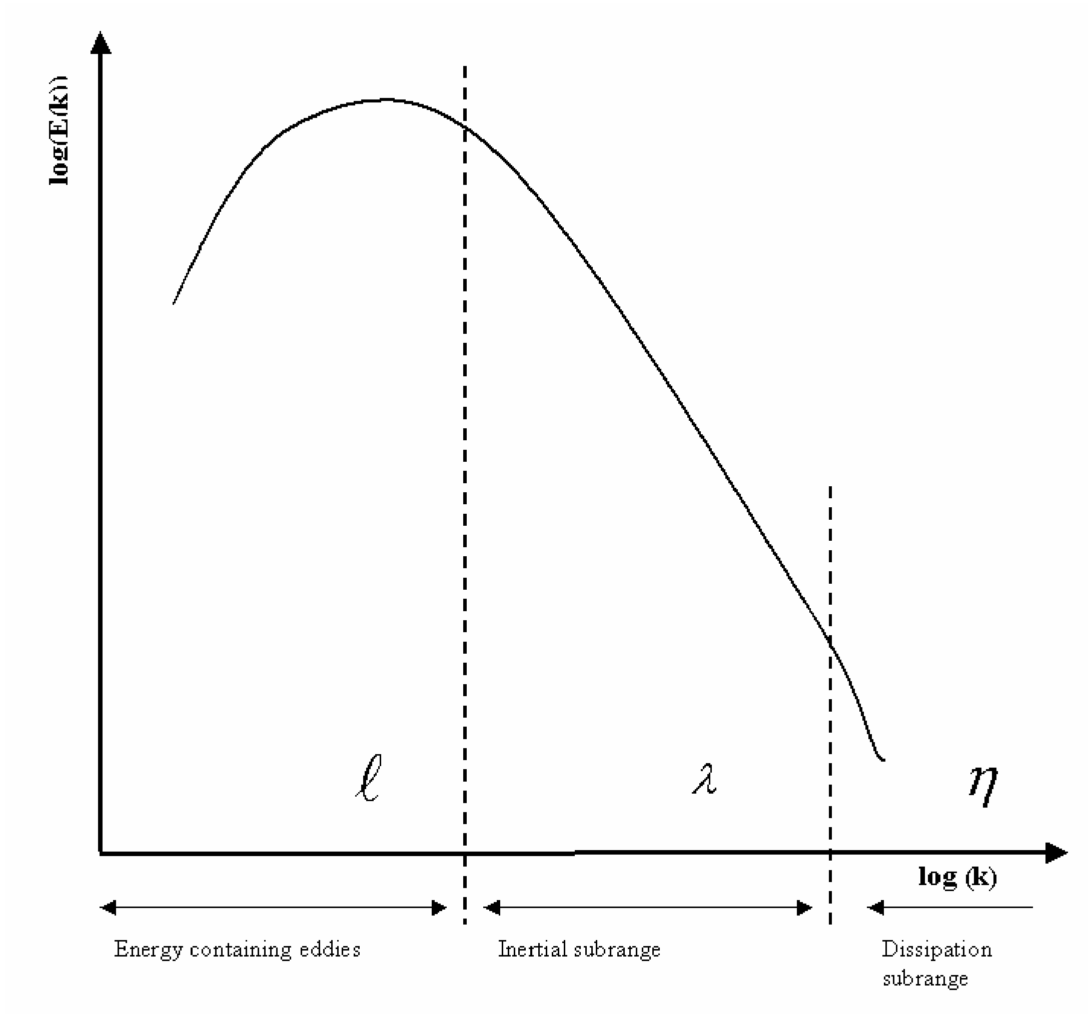

Figure 2.2: Turbulent kinetic energy spectrum

With the existing computer power, it is impossible to resolve all the length and time scales in complex flow geometries. According to the goal of the simulation, some models are needed to resolve turbulence.

In the derivation of uRANS equation, the exact flow variables, (for example the exact flow velocity $u(x,t)$ is split into a time average $\overline{u}^{T}(x,t)$ and a turbulent fluctuation term $u'(x,t)$. The first term represents the coherent structure of the flow and it is solved directly from the uRANS equations. The second on the other hand represents the turbulent part of the flow and it is modeled. Since this is an unsteady approach, it contains more information than RANS, but it still precludes a deterministic description of a particular event. The decomposition of the energy spectrum with uRANS approach can symbolically be presented as follows.

LES formulation depends on the idea of splitting the exact turbulent motion into large and small structures. The structures with large length scales, i.e. large eddy, are resolved with the LES and the rest is modeled.

Although it is well known (clearly seen in the energy spectra decomposition) that the formulation of LES is more accurate than the formulation of the Reynolds Averaged Navier Stokes equations, still uRANS is preferred in many applications. A major advantage of uRANS with respect to LES is that it can predict the flow data with some degree of accuracy in relatively coarser grids, thus the computational resource and CPU-time requirements are much less than that required by LES. Today, uRANS is affordable with the state of the art personal computers and therefore it is suitable for many industrial applications. But for applications where more accuracy is required, it is still not satisfactory. Especially for acoustics, where the small scales of turbulence determine the characteristics of sound, the deterministic approach of uRANS is misleading. Experience shows that RANS overestimates the sound pressure level. Similar level of error is also introduced when Led resolution. Therefore, LES with an adequate grid resolution is a must for reliable noise prediction.

2.1.3. Large Eddy Simulation

Large Eddy Simulation (LES) makes use of the knowledge that the large structures of turbulence contain most part of the turbulent energy of the flow. Turbulent energy is transferred from large structures to smaller ones and it is finally dissipated through the smallest structures. Large structures are coherent, inhomogeneous and energetic, whereas small structures are isotropic, homogeneous and dissipative. The effect of the small structures is comparable to the viscosity. Therefore, it is a good approximation to resolve only the energetic ones and model the dissipative part instead of resolving the whole range of structures.

Large Eddy Simulation has become a major tool for studying turbulent flows and covers today a wide range of applications. In contrast with $k-\varepsilon$ based models, LES can handle not only non-isotropic turbulence, but also transitional flows and flows that contain coherent structures in addition to turbulence. Since the unsteadiness of the flow field is well captured, the dynamics of the acoustic sources are well represented.

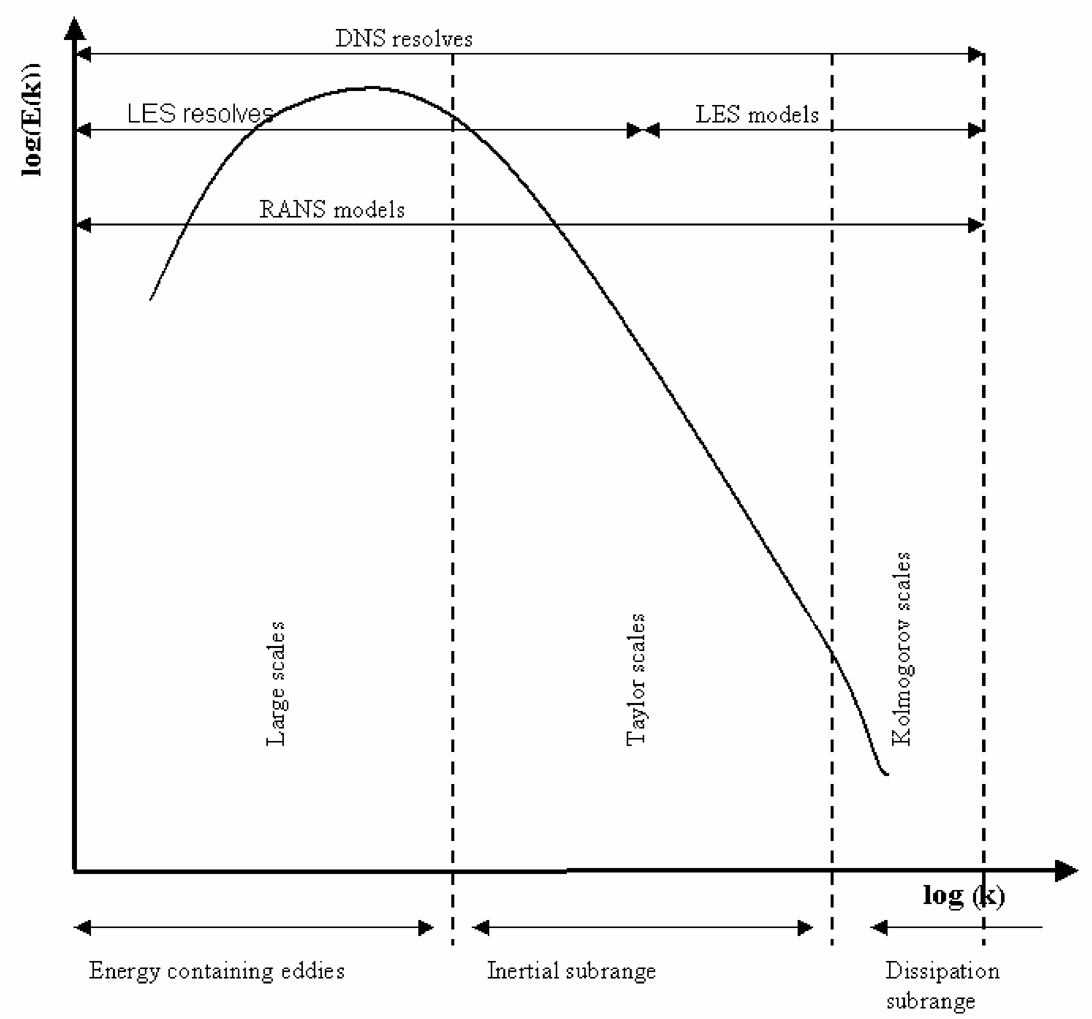

Figure 2.3: Turbulent scales resolved/modeled by RANS, LES and DNS.

Large Eddy Simulation is characterized by dividing the flow field into large and small scales by a filtering procedure. The large and energy-carrying scales of turbulence depend upon the geometrical configuration and the boundary conditions of the flow field. The smaller scales do not depend on the geometry and tend to be more homogeneous, universal and less affected by the boundary conditions.

While RANS approach (based on a time averaging of the flow field) models all the scales, LES resolves a large range of scales entering into the inertial subrange as shown in Fig. 2.3. This improvement represents a step towards Direct Numerical Simulation, where all the scales are resolved. In the LES only a small part of spectrum, represented by the small scales and their interaction with the resolved ones, has to be modeled. This is done by introducing a Subgrid-Scale (SGS) model. The small unresolved scales are called the subgrid scales.

First of all the SGS models is to account for the dissipative effects of the small scales which are filtered out. Secondly, the SGS terms have to account for the back-scatter phenomenon, which represents the effect of the small scales on the large ones.

For LES a spatial filtering procedure is employed instead of the temporal average used in deriving the RANS equations. Hence, the expression for the LES equations can be obtained if a filtering procedure in space (Favre spatial average) is applied to the governing equations, where the averaged variable is the resolved one. The resulting equations describe the evolution of the large eddies and contain the subgrid-scale stress (SGS) tensor.

The LES equations are derived from the original conservation laws of mass Eqn. (12), momentum Eqn.(13) and energy Eqn.(14) are:

$$\frac{\partial\overline{\rho}}{\partial t}+\frac{\partial\overline{\rho}\tilde{u}_i}{\partial x_i}=0 \tag{12}$$

$$\frac{\partial(\overline{\rho}\tilde{u}_i)}{\partial t}+\frac{\partial(\overline{\rho}\tilde{u}_i\tilde{u}_j)}{\partial x_j}=-\frac{\partial\overline{p}}{\partial x_j}+\frac{\partial}{\partial x_j}(\overline{\sigma_{ij}}+\tau_{ij}^{SGS}) \tag{13}$$

$$\frac{\partial(\overline{\rho}\tilde{h})}{\partial t}+\frac{\partial(\overline{\rho}\tilde{u}_j\tilde{h})}{\partial x_j}=\frac{\partial\overline{p}}{\partial t}+\frac{\partial}{\partial x_j}\left(\overline{\frac{\mu}{\Pr}\frac{\partial h}{\partial x_j}}\right)+\frac{\partial}{\partial x_j}(\overline{-\rho h''u''_j}) \tag{14}$$

The system is completed by the filtered equation of state:

$$\overline{p}=R_{gas}\overline{\rho}\tilde{T} \tag{15}$$

The molecular viscous stress tensor ($\overline{\sigma_{ij}}$) is obtained using the filtered velocity:

$$\overline{\sigma_{ij}}=\overline{\mu}\left[\frac{\partial\tilde{u}_i}{\partial x_j}+\frac{\partial\tilde{u}_i}{\partial x_i}-\frac{2}{3}\left(\frac{\partial\tilde{u}_k}{\partial x_k}\right)\delta_{ij}\right] \tag{16}$$

The subgrid stress tensor (τ_{ij}^{SGS}) is defined as:

$$\tau_{ij}^{SGS} = -\bar{\rho}(u_i u_j - \tilde{u}_i \tilde{u}_j) \tag{17}$$

and it must be modeled by using a SGS model.

The computational effort required by LES can be estimated in terms of Reynolds number. Since LES resolves the large scales and models the small ones, the smallest resolved scale has to be situated in the inertial subrange of the turbulent kinetic energy spectra (see Fig. 2.3), where the scales are independent of the geometry. A measure of these scales is the Taylor microscale (λ). The number of grid points needed to resolve a three dimensional flow field, based on equation (18) is N_{pts} as given below:

$$N_{pts} \sim \left(\frac{l}{\lambda}\right)^3 \sim Re_t^{\frac{3}{2}} \tag{18}$$

where l is the integral length scale.

These scales have to be resolved also in time. The time step should resolve the scales which are similar in size to that of Taylor microscale. The number of time steps required is N_{ts}:

$$N_{ts} = \frac{t_1}{\Delta t} = \frac{l}{U}\frac{U}{h} \sim \frac{l}{\lambda} \sim Re_t^{\frac{1}{2}} \tag{19}$$

where t_1 is the integral time scale, Δt represents the time step, h is the cell size and U is the characteristic velocity. The total computational effort needed for LES can be roughly estimated by combining the requirements for space and time resolution ($Re^{3/2} \cdot Re^{1/2}$) which yields $O(Re^2)$. This is less than in the case of DNS $O(Re^3)$. The continuous development of computational resources also makes LES suitable for more and more complex turbulent flows.

2.1.4. Direct Numerical Simulation

Direct Numerical Simulation (DNS) resolves all scales of turbulence in both space and time, from the largest scale down to the Kolmogorov microscale. In this case there is no need for averaging the governing equations and therefore no turbulence model is required. The drawback of DNS is that in order to solve all the scales, a very fine grid resolution is necessary and thus very large memory requirements. One can derive an expression for the number of grid points required by DNS for an adequate resolution and a three dimensional computation:

$$N_{pts} \sim \left(\frac{l}{\eta}\right)^{3} \sim Re_t^{\frac{9}{4}} \tag{20}$$

The number of grid points increases rapidly with the Reynolds number in DNS. The time step that should be used in DNS must be based on Kolmogorov length scale and the integral velocity scale ($\Delta t = \eta / U$). The number of time steps can be estimated for DNS:

$$N_{ts} = \frac{t_l}{\Delta t} \sim \frac{t_l . U}{\eta} \sim \frac{l}{\eta} \sim Re_t^{\frac{3}{4}} \tag{21}$$

The total computational effort needed for DNS can be estimated by combining the requirements for space and time resolution, which yields O (Re^3). This makes the application of DNS possible for flow with relatively low Reynolds numbers and simple geometries.

2.1.5. Reynolds Averaged Navier-Stokes Equations

The simplest approach used to compute a turbulent flow field is based on a numerical solution of the Reynolds Averaged Navier-Stokes (RANS) equations with appropriate turbulence models. The RANS approach is based on a time averaging of the flow field. In the conventional Reynolds decomposition, a randomly changing flow variable (ϕ) can be replaced by a mean ($\overline{\phi}$) and a fluctuating part (ϕ') (see Fig. 2.4):

$$\phi = \overline{\phi} + \phi' \tag{22}$$

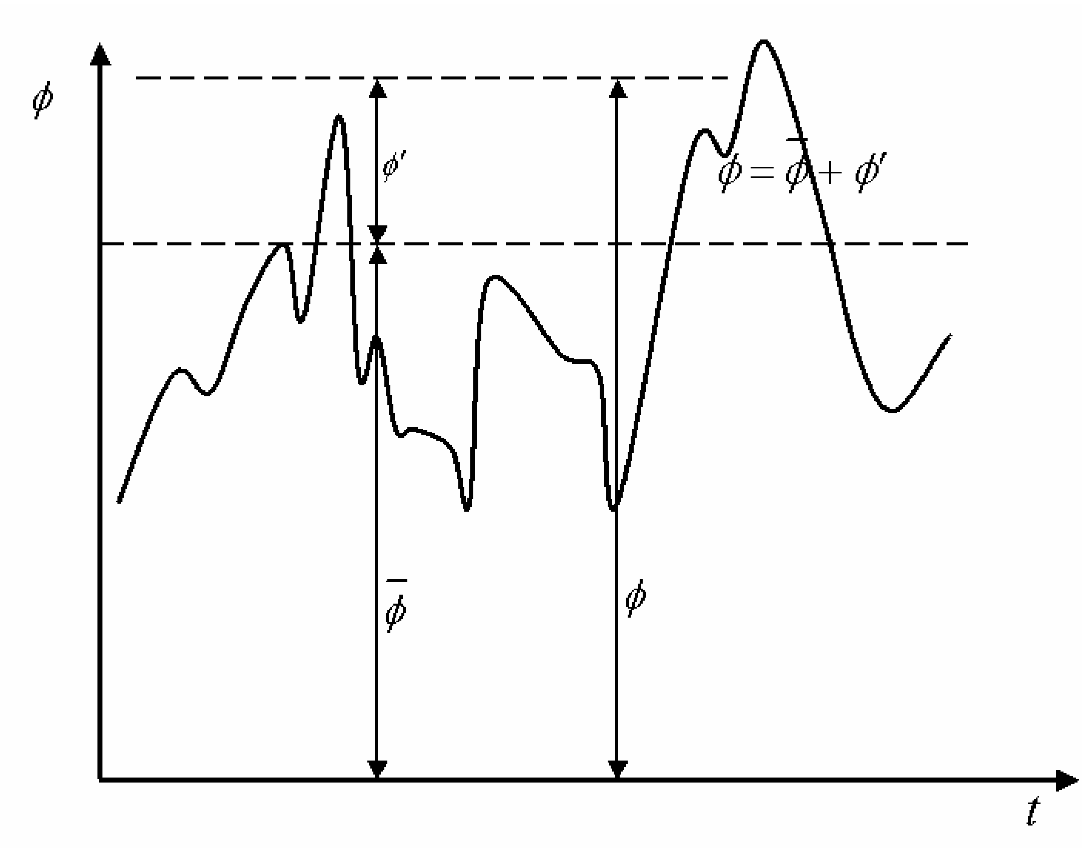

Figure 2.4: Time history of a variable in a turbulent flow field.

2.1.6. Algebraic Model

The algebraic model uses algebraic relationships in order to compute the eddy viscosity. No additional transport equation is involved. Prandtl proposed a mixing length model, where the eddy viscosity is computed by using:

$$\mu_T = C\mu\rho l_{mix}^{\ 2}\left|\left(\frac{\partial \overline{u_i}}{\partial x_j} + \frac{\partial \overline{u_j}}{\partial x_i}\right)\right| \qquad (23)$$

where C_μ is a model constant. Depending on the flow situation l_{mix} represents the mixing length given by an algebraic expression [36]. These models are simple, easy to implement, but are not general and require to be tuned for each case. Another drawback is that only local turbulence effects are considered, any remote effects that turbulence convection (history) can cause are neglected.

2.1.7. One Equation Model

In the one equation model an additional transport equation is introduced. Typically a transport equation for the turbulent kinetic energy is used. The turbulent kinetic energy (k) is defined as:

$$k = \frac{\overline{u_i' u_i'}}{2} \tag{24}$$

The velocity scale is approximated with $\sqrt{k}$ and the turbulent length scale is still computed by an algebraic expression. The eddy viscosity is then computed based on dimensional analysis as:

$$\mu_T = C_\mu \rho k^{1/2} l \tag{25}$$

This formulation presents some advantages in comparison with the algebraic model. However, due to the presence of an additional transport equation, the computational cost is higher.

2.1.8. Two-equation Model

The two-equation model involves two differential transport equations, which are used to estimate the turbulent velocity and length scales. Commonly one equation is a transport equation for the turbulent kinetic energy (k). For the second differential equation, different transported quantities are used. The second transported quantity can be the dissipation rate of turbulent kinetic energy ε ($k-\varepsilon$ models), the turbulent time scale τ ($k-\tau$ models) or the specific turbulent kinetic energy dissipation rate ω ($k-\omega$ models) [36].

The most widely used model in industry is the $k-\varepsilon$ model. The eddy viscosity is computed through:

$$\mu_T = C_\mu \rho \frac{k^2}{\varepsilon} \tag{26}$$

The two-equation model offers relatively accurate results and requires low computational costs in comparison with other, more complex (but more accurate) turbulence models. However, they fail to predict well those cases with adverse pressure gradient, anisotropy or high streamline curvature (swirling flows, impinging jets, flows with stagnation points and separation bubbles etc.). The deficiency of the model is attributed to its limited accuracy in predicting the Reynolds stresses. Since only information about the local mean flow is available, RANS lacks also a description of the unsteadiness of the flow field and hence cannot represent the dynamics of the acoustic sources well.

Another possible approach that can be used for handling the turbulent stresses is the Reynolds Stress Model (RSM). In the RSM approach a differential equation for each of the Reynolds stress tensor terms is solved. Additionally, a transport equation for the dissipation rate of the turbulent kinetic energy is necessary to close the system. The anisotropy and turbulence history effects are automatically considered in the RSM approach. However, the need to solve seven additional equations implies numerical difficulties and high computational costs.

2.2. Theory of the Sound

2.2.1. Basics

Sound pressure, p(t) is defined as the fluctuations overlapping the atmospheric pressure and emitted from certain sources. These pressure fluctuations can be caused by various mechanisms. Vibration of a solid body or turbulence in a flow and also heat sources can act as a sound generation mechanism. Examples of free fluid motion are the jets or the mixing layers. The main source of noise in these cases is the turbulence of the fluid generated by the shear-layers. [33]

After the emission, sound propagates in a waveform through the medium. Sound waves can be reflected, partially absorbed or attenuated. The sound waves, which are parallel to the direction of propagation, are called longitudinal waves. Whereas, the perpendicular ones are called lateral waves. Sound waves in fluids are waves of longitudinal type. [10]

A sound wave can have an arbitrary form. However, any periodic wave function can be defined as a superposition of harmonic signals with different amplitudes and frequencies.

A sound wave with distinct amplitude A and a distinct frequency f (in Hz) is called a pure tone and expressed as follows:

$$p(t) = A.\cos(2\pi f\ t) \tag{27}$$

Human ear can hear sound waves within a frequency range of about 16-16,000 Hz. Pressure fluctuations with lower frequencies are called infrasound and with higher frequencies ultrasound. Sound due to normal speech has frequencies in the vicinity of 1,000 Hz. Sensitivity of human ear to acoustic signal around that frequency is the highest.

A sound wave moves through a medium with the sound speed c, which is defined as:

$$c = \frac{\lambda}{T} \tag{28}$$

The wavelength λ is the distance between points of corresponding phase of two consecutive cycles of a wave and the period T is the elapsing time between two consecutive waves. Some common quantities used in acoustics are the angular frequency ω and the wave number k:

$$\omega = 2\pi f \tag{29}$$

$$k = \frac{2\pi}{\lambda} \tag{30}$$

$$c = \frac{\lambda}{T} = f\lambda = \frac{\omega}{k} \tag{31}$$

Normally, the propagation of sound waves in fluids is independent of the type or the origin of the sound signal. Sound speed is a property of the fluid and depends on the compressibility (K) and density (ρ) of the medium. Accordingly, the speed of sound in the dry air at 20°C is 343 m/s.

Human ear does not respond linearly to the amplitude of the sound pressure. The correspondence is rather logarithmic. Therefore, a logarithmic value, the Sound Pressure Level (SPL) is defined:

$$SPL = 10.log_{10}\left(\frac{p^2}{p^2{}_{ref}}\right) \tag{32}$$

whereas the reference pressure p_{ref} is mostly set as $2.0x10^{-5}$ Pa in air. The unit of the SPL is dB. SPL of the threshold of hearing is 0 dB and SPL of the threshold of pain is 140 dB. A loud conversation has a SPL of about 60 dB at the ear position. Note that SPL is a property of the field position. It does not only depend on the sound power of the source but also on the distance from the source, the directivity of the propagation and the properties of the medium. Time signal of a sound pressure is not sufficient to characterize the source of the sound. Since the amplitude and the frequency of the signal are determining the characteristics of the sound, the representation of the signal in the frequency domain is more insightful. Frequency analysis helps to distinguish the tonal components and the broadband swishing of the sound signal. Fourier Transformation is employed to transform the acoustic signal in the time domain into a function in the frequency domain. Modern acoustic measurement instruments include frequency analyzers which involve electronic filters to determine the SPL of the acoustic signal within given frequency bands. The frequency analyzers can be classified as constant bandwidth analyzers and octave analyzers. In the first group, each frequency band has the same width, ∇f . Narrow frequency bands allow determining the shape of the signal in great detail. The second group, octave analyzers are frequently employed in practice. Here, the ratio of the upper and lower frequencies, which bound the band, is fixed. The ratio is defined as $\sqrt[n]{2}$ for an $1/n$-octave band. Some of the common octave bands are the 1/1-octave, 1/3-octave and 1/12-octave bands. The octave spectra are preliminary used in the presentation of broadband signals with no prevalent frequencies.

Frequency spectra with higher resolutions can be transformed into a spectrum with a lower resolution. However, the reverse is not possible since the information content is not sufficient. For the transformation, all data points, SPLi, which lie within a frequency band of the coarser resolved spectrum, are added up.

$$SPL_{sum} = 10.log_{10}\left(\sum_{i=1}^{n} 10^{SPL_i / 10}\right) \tag{33}$$

The value $SPL_{ref.}$ is the sound pressure level of the corresponding frequency band in the coarse spectrum and n is the total number of the sound pressure levels within the coarse frequency band. Note that this transformation leads to an increase in the SPL. A SPL curve in the 1/3-octave spectrum has higher values in dB than the SPL-curve in the 1/12-octave spectrum of the same acoustic signal. The difference is minimal at the pure tones, but remarkable in the broadband distribution.

2.2.2. Wave equation

The wave equation has many physical applications from sound waves in air to magnetic waves in the Sun's atmosphere. Because of the various application fields, there exist different approaches for the derivation of the wave equation, for example by considering a stretched elastic string. Here, since the sound waves in fluids are of concern, the basic conservation laws of the fluid dynamics are used as the starting point.

$$\frac{\partial \rho}{\partial t} + \frac{\partial}{\partial x_i}(\rho u_i) = 0 \tag{34}$$

$$\frac{\partial}{\partial t}(\rho u_i) + \frac{\partial}{\partial x_i}(\rho u_i u_j - \tau_{ij}) + \frac{\partial p}{\partial x_j} = F_i \tag{35}$$

F_i represents the external forces and the shear stress τ_{ij} is defined as:

$$\tau_{ij} = \mu\left(\frac{\partial u_i}{\partial x_j} + \frac{\partial u_j}{\partial x_i} - \frac{2}{3}\delta_{ij}\frac{\partial u_k}{\partial x_k}\right) \tag{36}$$

The momentum equation can be simplified by assuming an inviscid fluid ($\mu = 0$), a uniform flow ($\partial(\rho u_i u_j) / \partial x_i = 0$) and the absence of the external forces ($F_i = 0$). This leads to

$$\frac{\partial}{\partial t}(\rho u_i) + \frac{\partial p}{\partial x_j} = 0 \tag{37}$$

By subtracting the divergence of the impulse equation (35) from the time derivative of the continuity equation the term $\partial^2(\rho u_i)/\partial t \partial x_i$ is eliminated.

$$\frac{\partial^2 \rho}{\partial t^2} - \frac{\partial^2 p}{\partial x_i \partial x_j} = 0 \tag{38}$$

The variables of an infinite, homogenous fluid can be linearized as $\rho = \rho_0 + \rho'$ and $p = p_0 + p'$. Here, the subscript 0 labels the properties of the steady background flow and ' labels the acoustic disturbances which overlie with the background flow. Substituting this linearization and the thermodynamic relationship $\partial p / \partial \rho = c_0^2$ for isentropic flows, the homogenous wave equation is achieved.

$$\frac{\partial^2 \rho'}{\partial t^2} - c_0^2 \frac{\partial^2 \rho'}{\partial x_i^2} = 0 \tag{39}$$

Propagation of a sound wave in a homogenous and motionless fluid is described with the homogenous wave equation (39). Note that the homogenous wave equation describes only the propagation of the sound waves; sound sources are not present in this equation. In the presence of a sound source, a source term Q is added to the right hand side of the equation (39). The inhomogeneous wave equation with a source term of order 2^n is written as follows.

$$\frac{\partial^2 \rho'}{\partial t^2} - c_0^2 \frac{\partial^2 \rho'}{\partial x_i^2} = \frac{\partial^n Q_{ij\ldots}}{\partial x_i x_{j\ldots}} \tag{40}$$

Green's formula is an appropriate method to solve this type of equations [38]. The solution of the generalized wave equation with the Green's formula is:

$$4\pi c_0^2 \rho'(\vec{x},t) = \frac{\partial^n}{\partial x_i \partial x_{j\ldots}} \int_{-\infty}^{\infty} Q_{ij\ldots} \frac{d\vec{y}}{r} \tag{41}$$

where r is the distance from the source. A sound source emerges when kinetic energy of the fluid is converted into acoustic energy. Such a conversion can take place by fluctuations of mass, momentum or strength. These are the elementary solutions of the wave equation, with sources of order 2^0, 2^1 and 2^2.

Mass fluctuations in the fluid generate sound sources of 1^{st} order, i.e. the monopole sources. Examples for this type of sound sources are a pulsating sphere, a diaphragm of a loudspeaker or volume displacement by a propeller blade. The 2^{nd} order source term is called a dipole and is generated due to a fluctuating momentum. This type of sound sources appear on the solid boundaries, due to vibration of solid bodies or varying aero dynamical force fields on the surfaces. The last elementary solution of the wave equation is the 4^{th} order source term, the quadrupole. Quadrupoles are strictly aero dynamical sound sources, generated due to the fluctuations in the flow field, e.g. due to turbulence. One important fact is that each type of the sound source is less efficient than the former one. The quadrupole source is the least efficient type of the sources. This statement gains more importance at low frequencies, or in other words at high wavelengths.

2.3. Lighthill

Lighthill's study on sound generated aerodynamically is a milestone in the aero acoustics [1,2]. He has introduced a methodology to compute the radiated sound depending on aero dynamical quantities. His work considered primarily the jet noise, without the effect of solid bodies affecting the generation or radiation of sound. Analog to the derivation of the wave equation, the starting point is the conservation laws of the fluid dynamics. The conservation of mass and momentum equations are used here in their original forms, i.e. without the assumptions of negligible viscosity and uniform flow. So, the neglected terms $\frac{\partial}{\partial x_i}(\rho u_i u_j - \tau_{ij})$ in the derivation of the homogenous wave equation are taken back into the account. Since the flow is unbounded, no external forces are present, i.e. $F_i = 0$. By introducing the identity:

$$c_0^2 \nabla^2 \rho = c_0^2 \frac{\partial^2 (\rho \delta_{ij})}{\partial x_i \partial x_j} \tag{42}$$

the inhomogeneous wave equation becomes:

$$\frac{\partial^2 \rho'}{\partial t^2} - c_0^2 \frac{\partial^2 \rho'}{\partial x_i^2} = \frac{\partial^n T_{ij}}{\partial x_i x_j} \tag{43}$$

where, T_{ij} is defined as:

$$T_{ij} = \rho u_i u_j + (p' - c_0^2 \rho')\delta_{ij} - \tau_{ij} \tag{44}$$

The equation (44) is known as the Lighthill's equation and T_{ij} as the Lighthill's tensor [1,2]. Note that, Lighthill's equation is the direct result of the conservation laws. No simplification is made during the derivation of the Lighthill's tensor; hence the equations of conservation of mass and momentum are valid for any arbitrary flow without external forces.

With the help of the Lighthill's equation, the sound field is deduced from the aerodynamic flow field. A back-reaction of the sound on the flow field is precluded. Fortunately, both theory and experiments show that the sound produced is so weak compared to the motions producing it, that no significant back-reaction can be expected, unless there is a resonator present to amplify the sound.

Lighthill's equation does not only cover the sound sources, but also the propagation of sound waves due to convection with the flow$(\rho u_i u_j)$, the propagation due to conduction of heat $(p' - c_0^2 \rho')$and the dissipation due to viscous effects(τ_{ij}). The dissipation of the acoustic energy due to viscosity is negligibly small in nearly all flows in practice. The term $(p' - c_0^2 \rho')$represents the deviation of the flow from the isentropic condition. This term gains importance where fast chemical reactions occur, such as combustion. Otherwise it is small and becomes zero for isentropic flows. Therefore, in most of the practical applications, the convection due to the flow is the dominating part in Lighthill's tensor and T_{ij} can be approximated to $(\rho u_i u_j)$. This approximation involves an error in the order ofM^2, since the pressure variations are proportional to the density fluctuations times the square of the sound speed$(p' \approx \rho' \cdot c_0^2 \approx M^2)$. Especially for low Mach number flows, Lighthill's tensor is in the order of the square of the mean flow velocity $(T_{ij} \sim u^2)$. The radiation field of the aero dynamical sound sources is however, proportional to the multiplication of the strength of the Lighthill's tensor and the square of the frequency of the acoustic signal. Theory and experiments show that the frequency of aerodynamic sound is proportional to the velocity of the mean flow, hence, the radiation of purely aerodynamic sound waves is in the order of the 8^{th} power of the mean flow, u^8 [2].

2.4. Solid Boundaries

Lighthill's acoustic analogy neglects the influence of the solid boundaries. Solid boundaries affect the aero dynamical sound field in two ways:

- The quadrupole sources generated aerodynamically are reflected or diffracted due to the solid boundaries.
- Additional sound sources are generated on the solid boundaries. These dipole sources are either due to the vibrations of the solid bodies or due to aero dynamical forces applied from the flow onto the boundaries.

Curle [4] has enhanced Lighthill's equation for stationary solid boundaries. Later, Ffowcs Williams and Hawkings have enhanced the formula further for moving solid boundaries [5]. In order to understand the effect of the moving solid boundaries on the acoustic field, let us consider an impermeable solid body positioned in a fluid flow enclosed by the surface S with the volume V (Fig. 2.5).

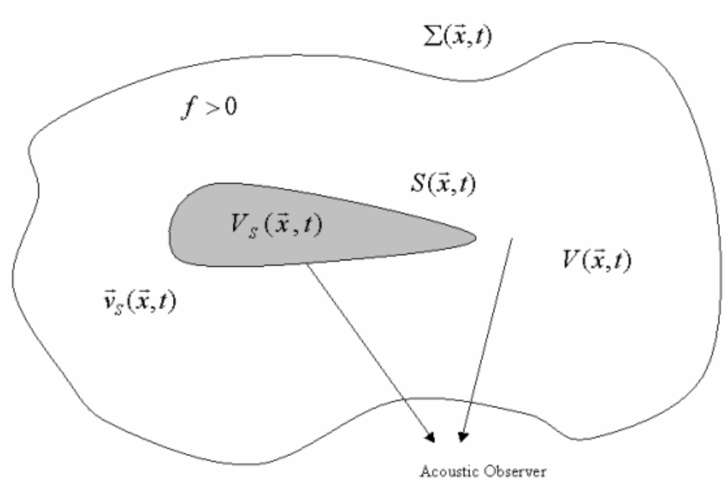

Figure 2.5: Acoustic analogy with moving solid bodies

The solid body has the volume V_S and its surface S is defined with a function $f(\vec{x},t)$. The surface is smooth, without discontinuities. It can move arbitrarily with the velocity $\vec{v}_S$ and change its shape and orientation.

$$f(\vec{x},t)\begin{cases} <0 & \text{in the solid body} \\ =0 & \text{on the solid body} \\ >0 & \text{outside the solid body} \end{cases} \tag{45}$$

Since the solid boundary is impermeable and the fluid is viscose, the fluid velocity on the boundary is equal to the velocity of the boundary, i.e. $f=0$ then $\vec{u}(\vec{x},t)=\vec{v}_S(\vec{x},t)$ and $\vec{u}(\vec{x},t)\cdot\vec{n}(\vec{x},t)=u_n(\vec{x},t)=0$, where $\vec{n}$ is the normal vector of the solid boundary directing outside. For this case, continuity and momentum equations are written as follows.

$$\frac{\partial\rho}{\partial t}+\frac{\partial}{\partial x_i}(\rho u_i)=\rho_0 v_{si}\delta(f)\frac{\partial f}{\partial x_i} \tag{46}$$

$$\frac{\partial}{\partial t}(\rho u_i)+\frac{\partial}{\partial x_i}(\rho u_i u_j-\tau_{ij})+\frac{\partial p}{\partial x_j}=p_{ij}\delta(f)\frac{\partial f}{\partial x_i} \tag{47}$$

where the compressive stress tensor is defined as $p_{ij}=p'\delta_{ij}-\tau_{ij}$ and dirac delta function is δ. Applying the same procedure as in Lighthill’s analogy, Ffowcs Williams and Hawkings equation is achieved.

$$\frac{\partial^2\rho'}{\partial t^2}-c_0^2\frac{\partial^2\rho'}{\partial x_i^2}=\frac{\partial^n T_{ij}}{\partial x_i x_j}-\left(p_{ij}\delta(f)\frac{\partial f}{\partial x_i}\right)+\left(\rho_0 v_i\delta(f)\frac{\partial f}{\partial x_i}\right) \tag{48}$$

In this equation two new terms appear in addition to the Lighthill’s equation, which are due to the presence and motion of solid bodies. The second term in the right hand side is called the loading noise. It represents the effects of the aero dynamical forces acting on the solid surface. Hence, it is a dipole source. The last term is called the thickness noise. The motion of the solid body in the fluid is the origin of this term. The volume displacement acts as a monopole sound source.

Until here, we have used a frame of reference, which moves with the sound sources. However, in numerous practical cases, the sound sources move with respect to the acoustic observer, like a moving aircraft or a propeller blade. Therefore, it is more convenient in practice to choose a frame of reference, which is stationary with respect to the acoustic observer. Let us define a coordinate system η, which is stationary with respect to the sound source and moving with respect to the observer with the velocity of the sound source, i.e. the velocity of the solid boundary $\vec{v}_s$.

The sound travels from the sound source at $\vec{y}$ to the observer at $\vec{x}$ with the speed of sound c_0 in a time of $\frac{|\vec{x}-\vec{y}|}{c_0}$. Within this time the origin of the coordinate system η travels a distance of $\vec{v}\cdot\frac{|\vec{x}-\vec{y}|}{c_0}=\vec{M}|\vec{x}-\vec{y}|$. If we assume that both coordinate systems coincide at a time t, then

$$\vec{\eta}=\vec{y}+\vec{M}|\vec{x}-\vec{y}| \tag{49}$$

$$\partial\eta=\partial y+(1-M_r) \tag{50}$$

where, M_r is the magnitude of the component of $\vec{M}$ in the direction of $\vec{r}=\vec{x}-\vec{y}$. The acoustic signal, which is emitted at the emission time τ_e is received by the acoustic observer at $t_{obs.}$.

$$\tau_e=t_{obs.}-\frac{|\vec{x}-\vec{y}|}{c_0} \tag{51}$$

If the new coordinate system is introduced into the Ffowcs Williams and Hawkings equation and Green's approach is employed to solve it, the following equation is achieved. Here, the brackets imply that the value inside belongs to the emission time τ_e.

$$
\begin{aligned}
4\pi c_0^2 \rho'(\vec{x},t) = {} & \frac{\partial^2}{\partial x_i \partial x_j} \int_V \left[\frac{T_{ij}}{r|1-M_r|} \right] d\eta \\
& - \frac{\partial}{\partial x_i} \int_S \left[\frac{p_{ij} n_j}{r|1-M_r|} \right] dS(\eta) \\
& - \frac{\partial}{\partial x_i} \int_{V_S} \left[\frac{\rho_0 \dot{v}_{si}}{r|1-M_r|} \right] d\eta \\
& - \frac{\partial^2}{\partial x_i \partial x_j} \int_{V_S} \left[\frac{\rho_0 v_{si} v_{sj}}{r|1-M_r|} \right] d\eta
\end{aligned}
\tag{52}
$$

Due to the far field approximation and rearrangements of the equation, the thickness noise in the equation (48) is split here into two terms, one containing the acceleration of the solid body, the other containing the surface velocity.

Since in practical applications, the acoustic signal at a large distance from the sound source is of interest, the far field approximation of the equation (52) gains importance. In order to carry out the far field approximation, let us first consider the spatial derivations of an arbitrary function $\phi(\vec{x},\tau)$, where τ represents the emission time variable:

$$
\begin{aligned}
\frac{\partial \phi}{\partial x_i} &= \left(\frac{\partial \phi}{\partial x_i} \right)_{\tau_e} + \left(\frac{\partial \phi}{\partial \tau} \right)_x \left(\frac{\partial \tau}{\partial x_i} \right) \\
&= \left[\frac{\partial \phi}{\partial x_i} \right] - \left(\frac{\partial \phi}{\partial \tau} \right)_x \frac{r_i}{c_0 r(1-M_r)}
\end{aligned}
\tag{53}
$$

If $\phi(\vec{x},\tau) = \dfrac{\varphi(\tau)}{r|1-M_r|}$, then

$$
\begin{aligned}
\frac{\partial \phi}{\partial x_i} &= \left[-\frac{\varphi r_i}{r^3} - \frac{r_i}{c_0 r(1-M_r)} \frac{\partial}{\partial \tau} \frac{\varphi}{r|1-M_r|} \right] \\
&= \left[-\frac{r_i}{c_0 r^2 (1-M_r)} \frac{\partial}{\partial \tau} \frac{\varphi}{|1-M_r|} \right] + O(r^{-2})
\end{aligned}
\tag{54}
$$

accordingly, second order spatial derivations can be evaluated as follows.

$$\frac{\partial^2\phi}{x_i\partial x_j}=\left[\frac{r_ir_j}{c_0^2r^3(1-M_r)}\frac{\partial}{\partial\tau}\frac{1}{(1-M_r)}\frac{\partial}{\partial\tau}\frac{\varphi}{|1-M_r|}\right]+O(r^{-2}) \tag{55}$$

If the terms falling off by $1/r^r$ are neglected for large values of the distance r and the function φ is replaced with the terms in the equation (52) $(\varphi=T_{ij},\varphi=f_i,\varphi=\rho_0\dot{v}_i)$ and $(\varphi=\rho_0v_iv_j)$, then the far field approximation of the Ffowcs Williams and Hawkings Equation is achieved.

$$\begin{aligned}\rho'(\vec{x},t)=&\frac{1}{4\pi c_0^4}\int_V\left[\frac{r_ir_j}{r^3(1-M_r)}\frac{\partial}{\partial\tau}\frac{1}{(1-M_r)}\frac{\partial}{\partial\tau}\frac{T_{ij}}{|1-M_r|}\right]d\eta\\&+\frac{1}{4\pi c_0^3}\int_S\left[\frac{r_i}{r^2(1-M_r)}\frac{\partial}{\partial\tau}\frac{f_i}{|1-M_r|}\right]dS(\eta)\\&+\frac{1}{4\pi c_0^3}\int_{V_S}\left[\frac{r_j}{r^2(1-M_r)}\frac{\partial}{\partial\tau}\frac{\rho_0\dot{v}_{si}}{|1-M_r|}\right]d\eta\\&+\frac{1}{4\pi c_0^4}\int_{V_S}\left[\frac{r_ir_j}{r^3(1-M_r)}\frac{\partial}{\partial\tau}\frac{1}{(1-M_r)}\frac{\partial}{\partial\tau}\frac{\rho_0v_{si}v_{sj}}{|1-M_r|}\right]d\eta\end{aligned} \tag{56}$$

The first term of the Ffowcs Williams and Hawkings (FWH) equation involves Lighthill's tensor and represents the purely aero dynamical sound sources which are mainly due to the turbulent fluctuations in the flow. This term is integrated over the whole fluid region. The second term in the right hand side represents the effect of the dipole sources at the solid surface, which are due to fluctuating aero dynamical forces on the boundary. The fluctuating aero dynamical force f_i consists of the fluctuations of pressure and viscose shear stress, $f_i=p_{ij}n_j=p\delta_{ij}-\tau_{ij}$. Lighthill has shown that the sound intensity of a quadrupole source is in the order of the 8^{th} power of the mean velocity. Similar reasoning shows that the intensity of a dipole source is proportional to the 6^{th} power of the mean flow velocity. These considerations result in the following proportionality of the sound intensities of the quadrupole and dipole sources, I_Q and I_D, respectively.

$$\frac{I_Q}{I_D} \sim \left(\frac{u}{c_0}\right)^2 = M^2 \tag{57}$$

At low Mach numbers the contribution of the dipole sources into the far field acoustic signal is larger than the contribution of the quadrupole sources. The radiation of the quadrupole sources is diminishing with respect to the radiation of the dipole sources. The acoustic efficiency η_a is defined as the ratio of the acoustic power output to the total energy supplied to the flow. Accordingly, the acoustic efficiency of the dipole sources is $\eta_{aQ} \sim M^3$, whereas the efficiency of the quadrupole sources is $\eta_{aQ} \sim M^5$.

The last two terms in Eq(56) represent the effect of the volume displacement. The moving solid body initiates dipole sources due to acceleration, $\rho_0 \dot{v}_{si}$ and quadrupole sources due to surface velocity, $\rho_0 v_{si} v_{sj}$. These sources are integrated over the volume of the solid body, which is equal to the volume of the displaced fluid due to the motion of the solid object. If the solid body is at rest, i.e. $v_s = 0$, then the FWH equation is reduced to Curle's equation, which is an enhancement to Lighthill's equation for stationary surfaces.

$$\begin{aligned}\rho'(\vec{x},t) = &\frac{1}{4\pi c_0^4}\int_V \left[\frac{r_i r_j}{r^3(1-M_r)}\frac{\partial}{\partial\tau}\frac{1}{(1-M_r)}\frac{\partial}{\partial\tau}\frac{T_{ij}}{|1-M_r|}\right]d\eta \\ &+\frac{1}{4\pi c_0^3}\int_S \left[\frac{r_i}{r^2(1-M_r)}\frac{\partial}{\partial\tau}\frac{f_i}{|1-M_r|}\right]dS(\eta)\end{aligned} \tag{58}$$

In the frame of this thesis the far field approximation of the FWH equation (56) is employed for the aerodynamic noise prediction. In what follows, the important characteristics of this method, its applicability, merits and limits will be discussed.

The accuracy of the predicted sound pressure level with FWH equation depends on the accuracy of the aero dynamical data which are used in the computation of the acoustic sources. The sound sources in FWH equation (52) are a direct result of the governing conservation equations. Since no simplification is made in the derivation, a perfectly accurate and detailed knowledge about the unsteady flow data would result in an exact computation of acoustic sources. Unfortunately, such a detailed knowledge on the flow field is almost impossible to achieve numerically or experimentally. The numerical errors in a flow simulation, which arise due to modeling, discretization and convergence, decrease the accuracy of the far field noise prediction.

An important property of the far field FWH equation is that a direct propagation of the sound waves from the sound source to the acoustic observer is assumed. The sound sources in the FWH equation are computed from the unsteady flow field. The computed sound sources are assumed to propagate directly to the acoustic observer along the distance vector $\vec{r}$ with the sound velocity c_0. This approximation is a logical consequence of Lighthill's considerations, where the sound waves are supposed to be generated in a turbulent flow and propagate undisturbed through a steady flow. The FWH equation is similar to Lighthill's equation in this aspect; its applicability is limited in the same manner. The far field FWH equation (Eqn. (56)) can only be applied to cases where no obstacles exist between the sound sources and the observer. An obstacle would reflect, diffract or absorb the sound waves, hence change the path of the sound wave. However, according to the equation (56), sound waves have to travel through the shortest way to the acoustic observer, i.e., through $\vec{r}$.

The term ($1 - M_r$), also called the Doppler factor, is present in the denominator of each term in the FWH equation. For subsonic flows this term is in the range of (0; 1]. For supersonic flows, it tends to zero when M_r approaches to 1 and becomes zero where $\theta = cos^{-1}(1/M)$. Small values of the Doppler factor increase the importance of the terms in the FWH equation extensively and if the Doppler factor becomes zero, then singularities occur. Under such circumstances the FWH equation does not provide a proper description of the sound field although it is still valid. In order to avoid difficulties at transonic or supersonic flows, a better description of the sound field has to be employed. Since, in the frame of this work, only low Mach number flows are handled, the FWH equation in the form represented in (56) is used. Aero Acoustic methods for supersonic flows will not be explained here; the works of Brentner, Ianniello and Farassat [40-41] provide insight on this subject.

In the light of these considerations, some examples, where the far field FWH equation can be employed for noise prediction are:

- Aeolian sound of wires or cylinders
- Airframe noise of an aircraft or automobile

- Noise of propellers, fans or helicopter blades (in subsonic regime)

On the other hand, the use of far field FWH equation is inappropriate for the noise prediction of internal flows, like in a duct, in a pump or inside an automobile. In such cases, the employed noise prediction method has to resolve the propagation of the sound waves as well as their generation. Near field acoustic methods, like Linearized Euler Equations are appropriate to employ in such cases.

One of the most important advantages of FWH equation is that all terms in the equation are physically meaningful. The quadrupole sources account for the nonlinear effects, such as turbulence in the flow. Loading noise represents the acoustic contribution of the force acting on the fluid in the presence of a solid surface. Thickness noise appears due to the motion of the solid body and can be determined completely by the geometry and kinematics of the body. Hence, each noise source appearing in the FWH equation is related to an aero dynamical process. Each term is independent and can be computed separately. This fact allows comparing the contribution of each noise source to the total acoustic signal detected by an observer in the far field. FWH formulation provides a detailed insight about the relationship between the aerodynamics of a flow and its acoustic response. This knowledge can be used for two purposes. Firstly, the dominant noise sources can be identified by comparing the values of the terms and this knowledge can be used for the purpose of noise reduction. Secondly, some of the terms, which are known to be diminishing in a particular application - for example quadrupole sources in a low Mach number flow - may be neglected, in order to reduce the required computational power and CPU-time. The first term of the far field FWH equation is the volume integral of the turbulent acoustic sources. This integral can easily be rewritten as a surface integral. If the integration surface is chosen as the boundaries of the computational domain, both integrations are equivalent. In numerous implementations of FWH equation, the surface integral formulation is preferred in order to spare computational power. Furthermore, the integration surface is usually chosen nearer to the solid boundaries instead of the boundaries of the computational domain. This application is justified with the fact that the quadrupole sources are the least important and the least effective sources. Accordingly, only the quadrupole sources inside the integration surface are taken into account and the rest is ignored. Provided that the ignored part of the turbulent noise sources have really a negligible contribution to the acoustic signal at the observer, then the position of the integration surface does not falsify the acoustic computation. Note that in other acoustic methods, like Kirchhoff's analogy, the integration surface has to be positioned carefully in order to prevent numerical instabilities. Fortunately, the mathematical formulation of FWH equation is stable and such instabilities do not occur [44]. However, recent researches [45] indicate that the effect of the turbulent quadrupole sources on the total acoustic signal may be important, especially if a high order of accuracy in the acoustic prediction is required. Errors in the noise prediction, which are due to the limits of the integration domain, can be eliminated by computing the acoustic contribution of the whole computational domain. In the simulations carried out in this thesis, the volume integral of the quadrupole sources through the whole computational domain is computed in order to avoid errors due to a priori assumptions.

Another advantage of the FWH formulation is the robustness of the formulation. The computation of FWH equation is numerically robust and straightforward. Furthermore, its requirements of computational power and CPU-time are relatively low.

3. COMPUTATIONAL ANALYSIS

3.1. Computational Fluid Dynamic Analysis

The numerical simulations carried out in the frame of this thesis are performed with the flow solver FLUENT. In this chapter an overview of the numerical code is given. Important features of the code, which affect the quality of the aerodynamical solution and hence the accuracy of the acoustical prediction, are also discussed briefly.

The starting point in Computational Fluid Dynamics (CFD) is the mathematical model which describes the physical phenomena. The mathematical model may deviate from the real fluid dynamics due to various assumptions like inviscid fluids or incompressible flows. Such assumptions are well suited for some practical applications and simplify the mathematical model, and the simulation procedure extensively.

FLUENT can compute turbulent flows with Direct Numerical Simulation (DNS), Large Eddy Simulation (LES) or Reynolds Averaged Navier Stokes (RANS) equations. Turbulent flows involve a wide range of length and time scales. DNS is based on the idea to solve the unsteady Navier Stokes equations without any simplification in the mathematical model. So the whole kinetic energy dissipation is captured by resolving the smallest structures with Kolmogorov scale as well as the large structures with the integral scale of turbulence. For such a resolution, computational domain must be resolved with about $Re^{9/4}$ control volumes. Since the time step is proportional to the grid size, the cost of a DNS becomes Re^3. This is an unaffordable cost for most of the practical applications. LES on the other hand decreases the computational cost by resolving only the large, energetic scales of the flow and modeling the small, dissipative structures. Structures with larger length scales than the grid size are resolved. Hence, the required number of control volumes depends on the size of the minimum length scale which has to be resolved. Even though LES is cheaper in terms of computational power and CPU-time with respect to DNS, it is still expensive for most of the industrial applications where a coarse prediction of mean flow variables is often desired. RANS is appropriate whenever a quick estimation of the flow is desired and detailed information about the fast processes is unnecessary. In this model the governing equations are averaged in time and the terms containing the turbulent fluctuations (Reynolds stress) are modeled. The whole range of time and length scales are modeled. Due to this modeling, information about turbulent fluctuations gets lost. If the averaging is performed over a restricted time, unsteady RANS (uRANS) equations are achieved instead of the steady state RANS equations. uRANS allows temporal fluctuations in the flow. However, some information about the turbulence gets lost due to modeling of the Reynolds stress terms.

FLUENT allows users to choose one of two numerical methods:

- ❑ segregated solver
- ❑ coupled solver

Using either method, FLUENT will solve the governing integral equations for the conservation of mass and momentum and (when appropriate) for energy and other scalars such as turbulence. In both cases a control-volume-based technique is used that consists of:

- ❑ Division of the domain into discrete control volumes using a computational grid.
- ❑ Integration of the governing equations on the individual control volumes to construct algebraic equations for the discrete dependent variables such as velocities, pressure, temperature and conserved scalars.
- ❑ Linearization of the discretized equations and solution of the resultant linear equation system to yield updated values of the dependent variables.

The two numerical methods employ a similar discretization process (finite-volume), but the approach used to linearize and solve the discretized equations is different in each solver.

3.1.1. Segregated solution method

Using this approach, the governing equations are solved sequentially (i.e., segregated from one another). Because the governing equations are non-linear (and coupled), several iterations of the solution loop must be performed before a converged solution is obtained. Each iteration consists of the steps illustrated in Figure 3.1 and outlined below:

1. Fluid properties are updated based on the current solution. (If the calculation has just begun, the fluid properties will be updated based on the initialized solution.)

2. The u, v and w momentum equations are each solved in turn using current values for pressure and face mass fluxes in order to update the velocity field.

3. Since the velocities obtained in step 2 may not satisfy the continuity equation locally, a Poisson-type equation for the pressure correction is derived from the continuity equation and the linearized momentum equations. This pressure correction equation is then solved to obtain the necessary corrections to the pressure and velocity fields and the face mass fluxes such that continuity is satisfied.

4. Where appropriate, equations for scalars such as turbulence, energy and radiation are solved using the previously updated values of the other variables.

5. When interphase coupling is to be included, the source terms in the appropriate continuous phase equations may be updated with a discrete phase trajectory calculation.

6. A check for convergence of the equation set is made.

These steps are continued until the convergence criteria are met.

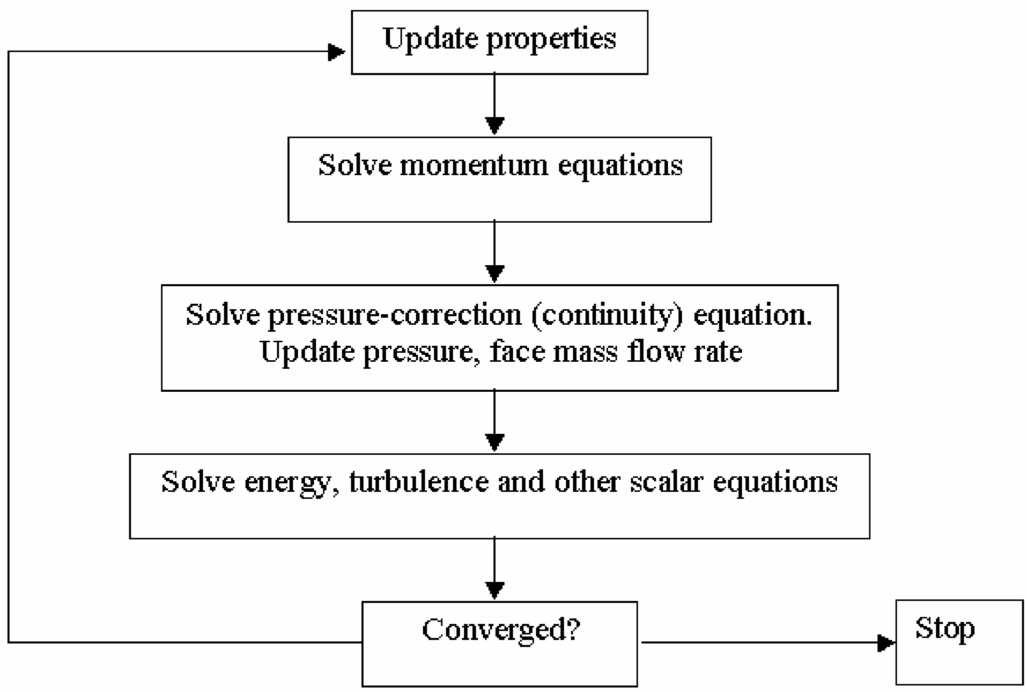

Figure 3.1: Overview of the Segregated Solution Method

The second step in CFD is the discretization of the mathematical model, in other words approximation of the differential equations by a system of algebraic equations which are functions of flow variables at some set of discrete locations in space and time. The CFD code FLUENT is based on the Finite Volume Method (FVM). The computational grid is hybrid – block structured around radial fan and unstructured mesh in volute and pipe. In FLUENT, spatial discretization can be carried out with 1^{st} or 2^{nd} order accurate methods. In the frame of this thesis, second order central differencing scheme is employed for the spatial discretization.

Time discretization can be carried out with explicit or implicit discretization schemes. In FLUENT both methods are implemented since each is optimal for different type of problems. In explicit schemes, the unknown variables of the next time step are described as functions of known variables from previous time steps. Therefore, explicit time discretization schemes have the advantage of computing the variables of the next time step with only one binary operation. On the other hand, implicit schemes describe the variables of next time step as a function of variables belonging to previous and future time steps. Therefore, an iterative procedure is required for the solution of an implicit scheme. The so-called inner iterations are carried out at each time step. This means that, for the same size of the time step, implicit methods require more operations, hence. more CPU-time than explicit ones. On the other hand, the disadvantage of explicit schemes is their stability limit. The explicit time step has to be set according to this stability condition in order to achieve a stable numerical computation. Implicit methods are, on the contrary, unconditionally stable. If the time step is set too large, then they result in a steady state solution. Thus, implicit schemes provide a high degree of freedom in the decision of the size of the time step. It is suggested to make use of this freedom whenever the smallest interested time scale is about two times larger than the temporal step size allowed for the explicit scheme. Under circumstances, implicit time discretization may reduce the required CPU-time for a computation remarkably without decreasing the accuracy of the unsteady solution.

FLUENT is designed for the simulation of practical problems where usually high Reynolds number flows in complex geometries are of concern. Under such circumstances flow is usually unsteady and the required number of control volumes is very high. Proportional to the number of control volumes, the required memory space and CPU time increase. In practice, one processor does not suffice. FLUENT is parallelized to overcome this problem with the Message Passing Interface (MPI). Blocks are distributed among the available processors. Load distribution is a criterion to describe the efficiency of parallelization, which is defined as the ratio of the maximum computational load of a processor to the minimum load of a processor. A load distribution of 1.0 is optimum, which means that all processors have the same amount of computations to handle. Low load distributions result in inefficient parallel computations.

3.2. Test Case: Radial Fans

3.2.1. Flow properties

Flow around fans has always attracted great attention of researchers from both aero dynamical and acoustical fields. In aero dynamical point of view, the flow around rotating bodies is challenging because of their highly complex flow structures. From an acoustician's point of view, the inheritance of both tonal and broadband noise components makes the aerodynamic sound of radial fans interesting.

Although analytical or semi-empirical methods are also employed for the noise prediction of radial fans, computational noise prediction methods are of special interest because of their high accuracy and capability of providing detailed information. In recent studies, computational Aero Acoustic methods are employed to investigate the trailing edge noise or the noise generation by the rotor stator interaction [11]. The noise generation mechanisms in axial flow machinery can basically be summarized in four points; blade interactions with inflow turbulence, turbulent boundary layer, tip clearance vortex and blade stall. The noise of a fan consists of tonal and broadband components. Tonal noise is the periodic part of the acoustic signal. The mechanism of the tonal noise can be understood by considering a fixed point in space near the blades. The forces acting on that point change periodically every time a pressure field is passing by, which initiated by a blade. Therefore, a discrete frequency noise is generated at the blade passing frequency and at the multiples of it, i.e., harmonics.

The broadband noise is due to the non-periodic fluctuations, mainly caused by turbulence. The turbulent boundary layer is one of the origins of the broadband noise. Another origin is the vortex shedding on the trailing edge of the blade. Another source for the broadband noise is the turbulent inflow which causes non-periodic fluctuations on the hub and the blades. Here, the geometry includes fan inside a volute, the disturbances in the inflow are very important.

The most important noise source in a fan is the dipole sources. The monopole sources which are originated by the volume displacement and act as a tonal noise, are negligible for flow with Mach numbers less than 0.6. The quadrupole sources, which are emitted by the volume sources away from the solid surfaces and inherit the characteristics of the broadband noise, are negligible as long as the Mach number remains less than 0.8.

Two radial fan system with their volute and inlet and outlet pipes are investigated. The first radial fan system- called ”FAN I” has a higher sound pressure levels than the radial fan system called “ FAN II”.

Nowadays, the state of the art computers are able to simulate even the complicated geometry of flow machines. However, if a simulation with high quality is desired, then the limits of the computer capacity are easily reached. LES has to be performed to achieve a satisfactory noise prediction. LES increases the accuracy of the simulation, but unfortunately also the computational requirements extensively.

Isometric 3D models for the volute and radial fan for “FAN I” are given in Fig. 3.2.

Figure 3.2: 3D model of the FAN I

The location of the fan inside the volute is given in Fig. 3.3. The tests and numerical simulations have been made on a centrifugal fan driven by a motor rotating at 2800 rpm. The radial fan has 37 forward curved blades with outlet diameters of 130 mm. The minimum distances between the impeller and the volute tongue are respectively small. Fig. 3.3 shows a cut-sketch of the fan-volute.

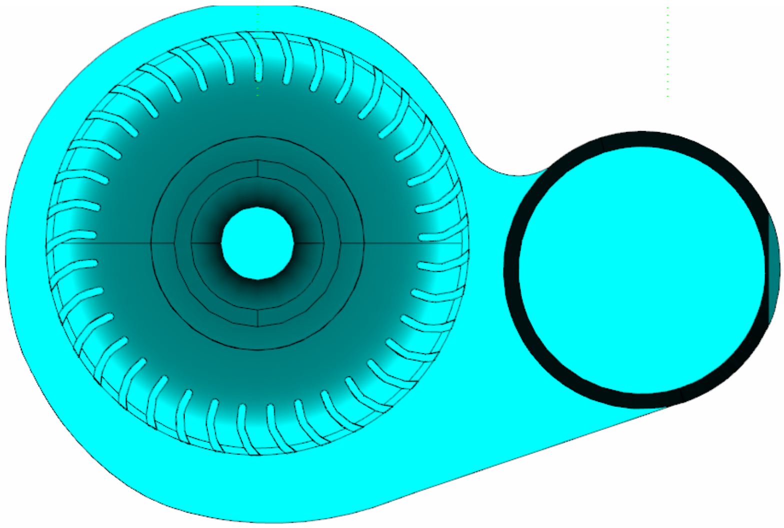

Figure 3.3: Detailed view of the fan-volute

Isometric 3D models for the volute and radial fan for "FAN II" are given in Figure 3.4.

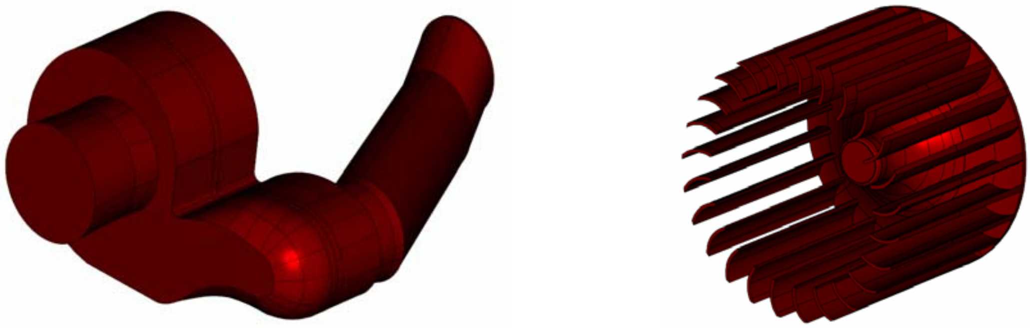

Figure 3.4: 3D models of "FAN II"

The location of the fan inside the volute is shown in Fig. 3.5. The tests and numerical simulations have been made on a centrifugal fan driven by a motor rotating at 2800 rpm. The radial fan has 25 forward curved blades. The minimum distances between the impeller and the volute tongue are respectively large. Fig. 3.5 shows a cut-sketch of the fan-volute.

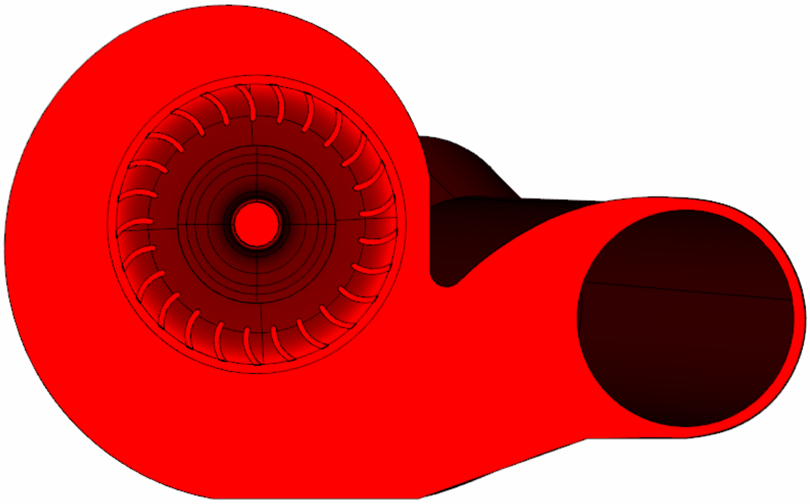

Figure 3.5: Detailed view of the fan-volute of FAN II

Summary of the technical specifications of the two different designs are given in Table. 3.1.

Table 3.1: Technical information of two designs

	FAN I	FAN II
Fan Outer Dia. [d]	130 mm	120 mm
Fan Depth [b]	55 mm	85 mm
Number of Blades [z]	37	25
Fan Speed	2800 rpm	2800 rpm

3.2.2. Numerical details

The employed boundary conditions are no-slip at the walls, Pressure Inlet and Pressure Outlet. Pressure inlet boundary conditions are used to define the fluid pressure at flow inlets, along with all other scalar properties of the flow. They are suitable for both incompressible and compressible flow calculations. Pressure inlet boundary conditions can be used when the inlet pressure is known but the flow rate and/or velocity is not known.

Pressure outlet boundary conditions require the specification of a static (gauge) pressure at the outlet boundary. The value of the specified static pressure is used only while the flow is subsonic. A set of "backflow" conditions are also specified should the flow reverse direction at the pressure outlet boundary during the solution process. Convergence difficulties will be minimized if realistic values for the backflow quantities are specified.

Flow over fans can exhibit asymmetries; propellers with fewer blades tend to cause more asymmetries in the flow. In order to capture any possible asymmetries in the flow, the whole fan-volute geometry is simulated. Any symmetry or periodicity assumptions are omitted.

LES and uRANS are performed to simulate the flow around cylinder. Spatial discretization is performed with the 2nd order central differencing scheme. This implicit method is preferred to explicit methods because of CPU-time considerations. In contrary, implicit methods allow larger time steps and shorten the required CPU-time massively.

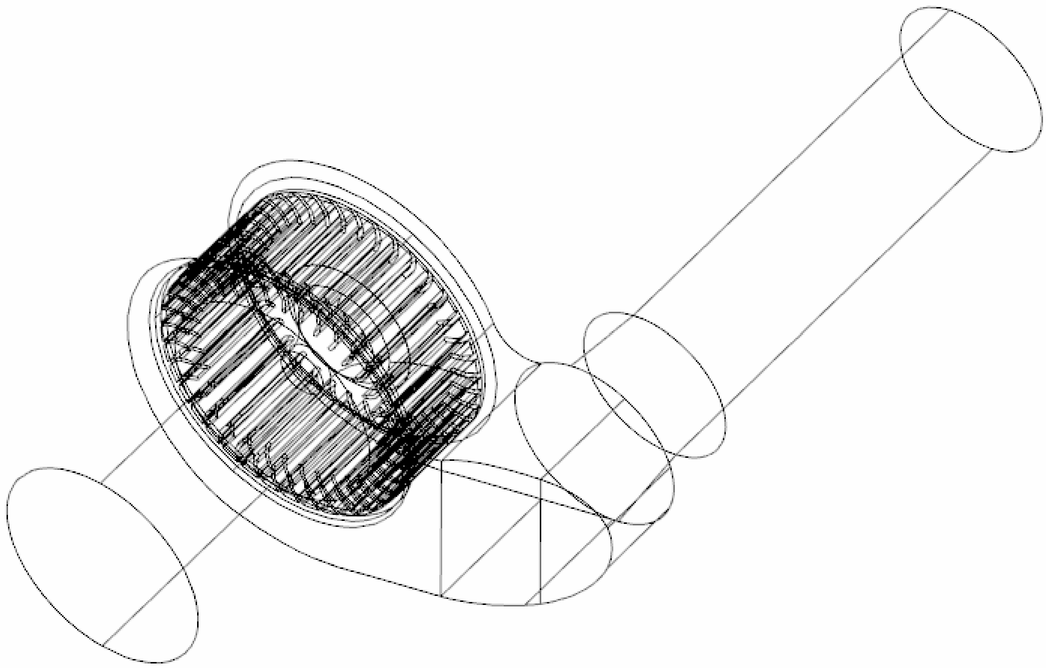

Figure 3.6: Flow domain of FAN I

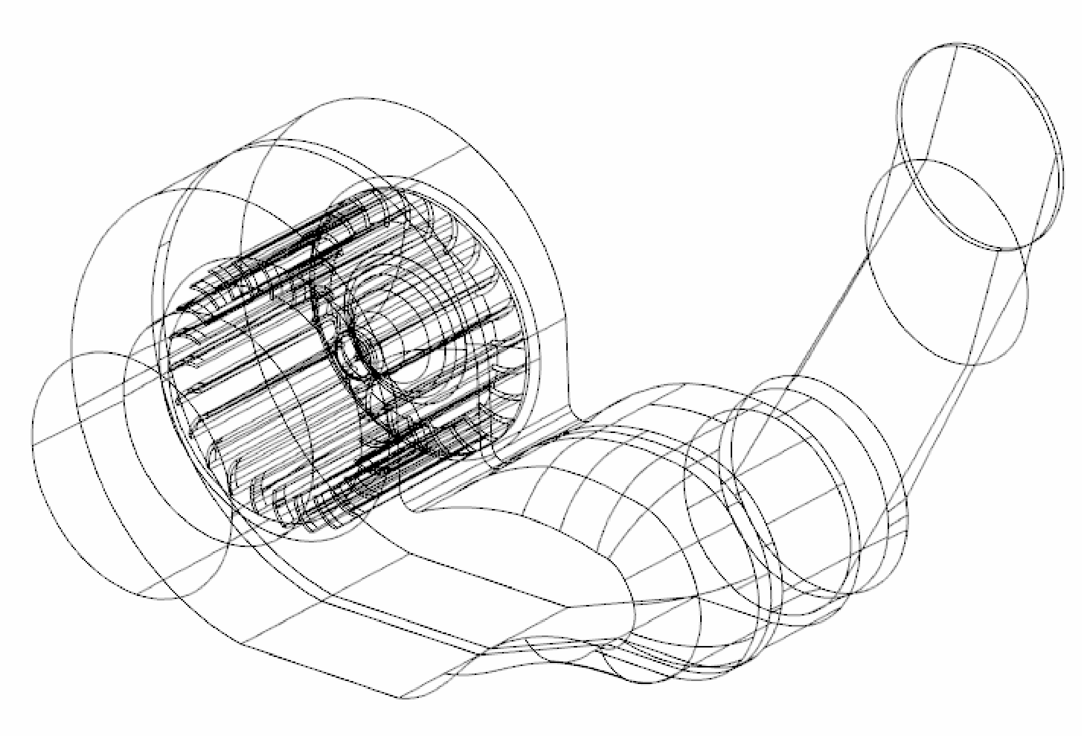

Figure 3.7: Flow domain of FAN II

The computational mesh for new and current design involves approximately $2.5.10^6$ control volumes. A detailed view of the mesh is shown in the Fig. 3.8. Cell distribution is forced to be finer on the walls to resolve the boundary layer and in the neighborhood of the blade. The dimensionless wall distance y+ is kept about 1 over the whole propeller surface and the use of a wall model is omitted.

3.2.3. Sliding meshes

When a time-accurate solution for fan-casing interaction (rather than a time-averaged solution) is desired, one must use the sliding mesh model to compute the unsteady flow field. The sliding mesh model is the most accurate method for simulating flows in multiple moving reference frames, but also the most computationally demanding.

Most often, the unsteady solution that is sought in a sliding mesh simulation is time periodic. That is, the unsteady solution repeats with a period related to the speeds of the moving domains. However, one can model other types of transients, including translating sliding mesh zones.

When transient fan-casing interaction is desired one must use *sliding meshes*. If one is interested in a steady approximation of the interaction, then using the *multiple reference frame* model may be better.

In this study, multiple reference frame model is used for steady simulation, with $k-\varepsilon$ turbulence model. After convergence is achieved, then sliding mesh is model used for transient analysis with LES turbulence model.

The computation is carried out with discretization methods of second order accuracy both in time. The time step is set to 1×10^{-4} s, which means about 1° of rotation of fan per time step.

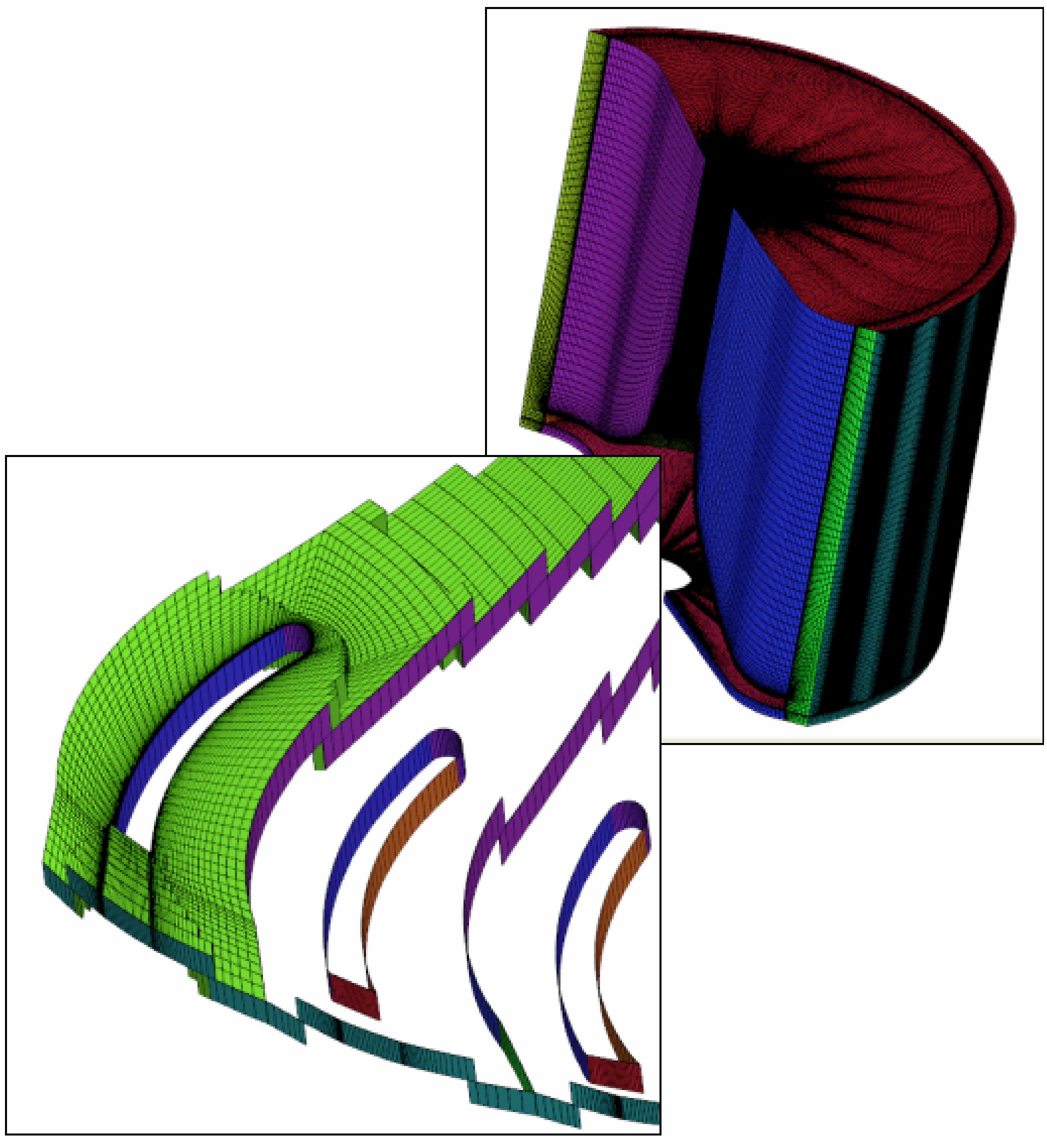

Figure 3.8: Computational grid

3.2.4. Results

Following figures aim to give an overview of the flow around the fan and inside the volute.

Fig. 3.9 shows the instantaneous picture of the magnitude of the vorticity at a cross-section along the flow domain. The vorticity is produced mainly at the tip, on the suction side of the blades and on the hub. It is then transported further with the flow through the pipe. From figures it can be seen that the FAN II produce less vorticity in comparison with the FAN I. The color scales are the same for two fans.

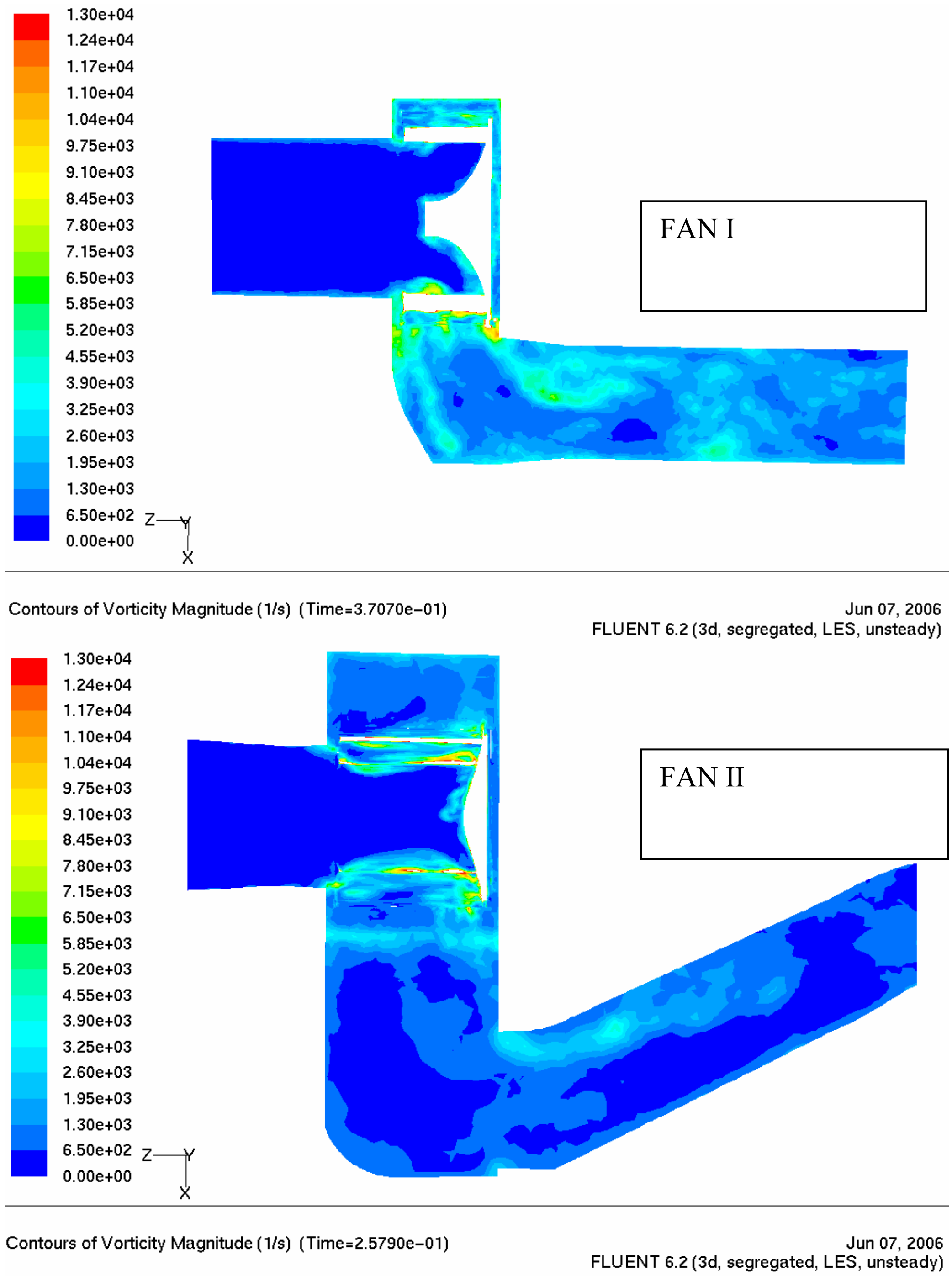

Figure 3.9: Instantaneous picture of the magnitude of the vorticity

Fig. 3.10 shows the instantaneous picture of the magnitude of the velocity at a cross-section along the flow domain. The flow in FAN I is highly disturbed and transported helically along the pipe. On the contrary to FAN I, FAN II has a smooth velocity distribution along the volute and pipe.

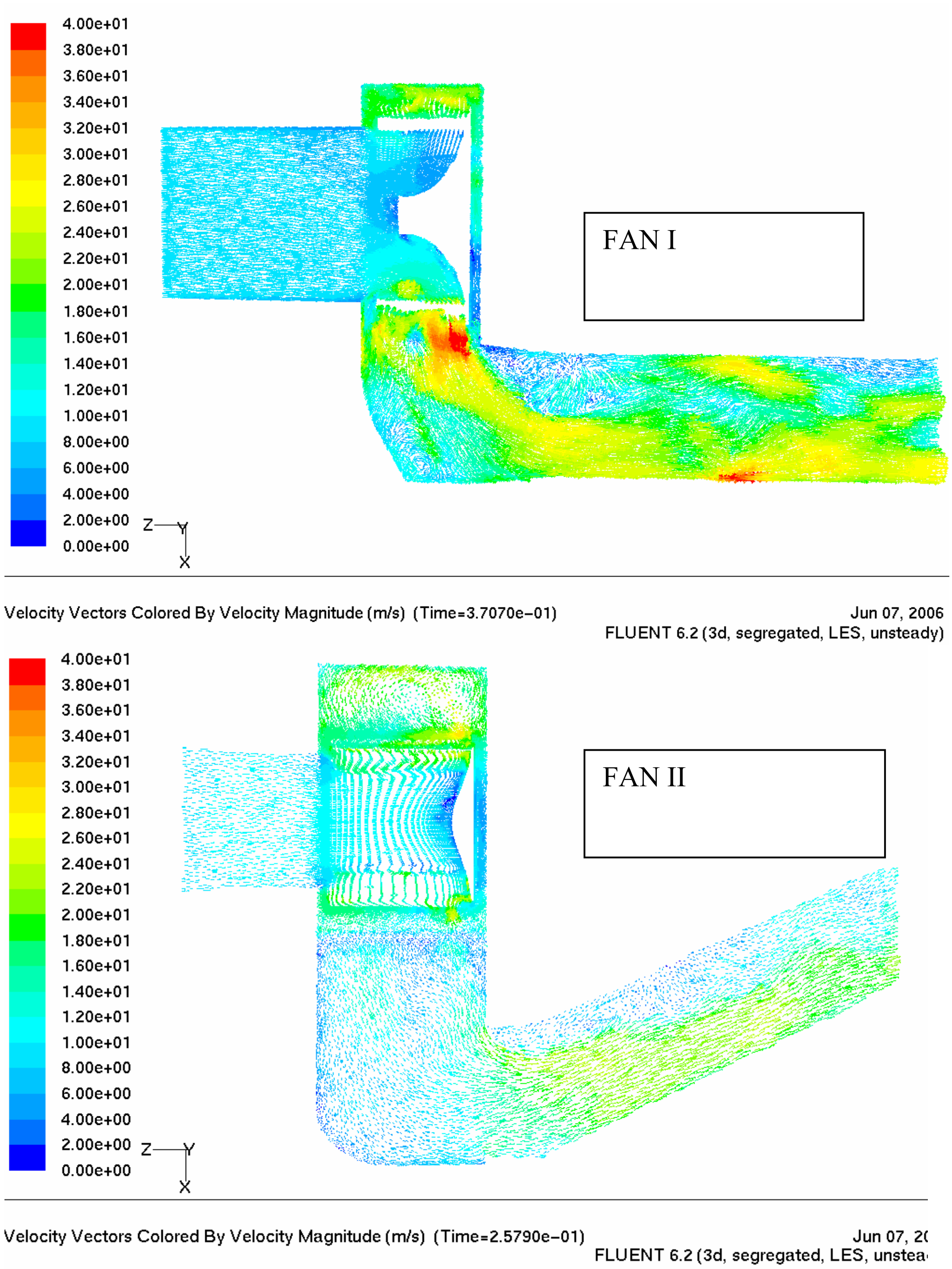

Figure 3.10: instantaneous picture of the magnitude of the velocity

Fig. 3.11 shows the instantaneous pressure distribution on the volute and pipe of two designs. FAN II shows smooth pressure increase along the volute and the magnitudes are lower in comparison with the FAN I. FAN I has pressure decrease while the volute-fan clearance increasing. Another sudden change in the pressure is visible at the pipe-volute interface in the FAN I.

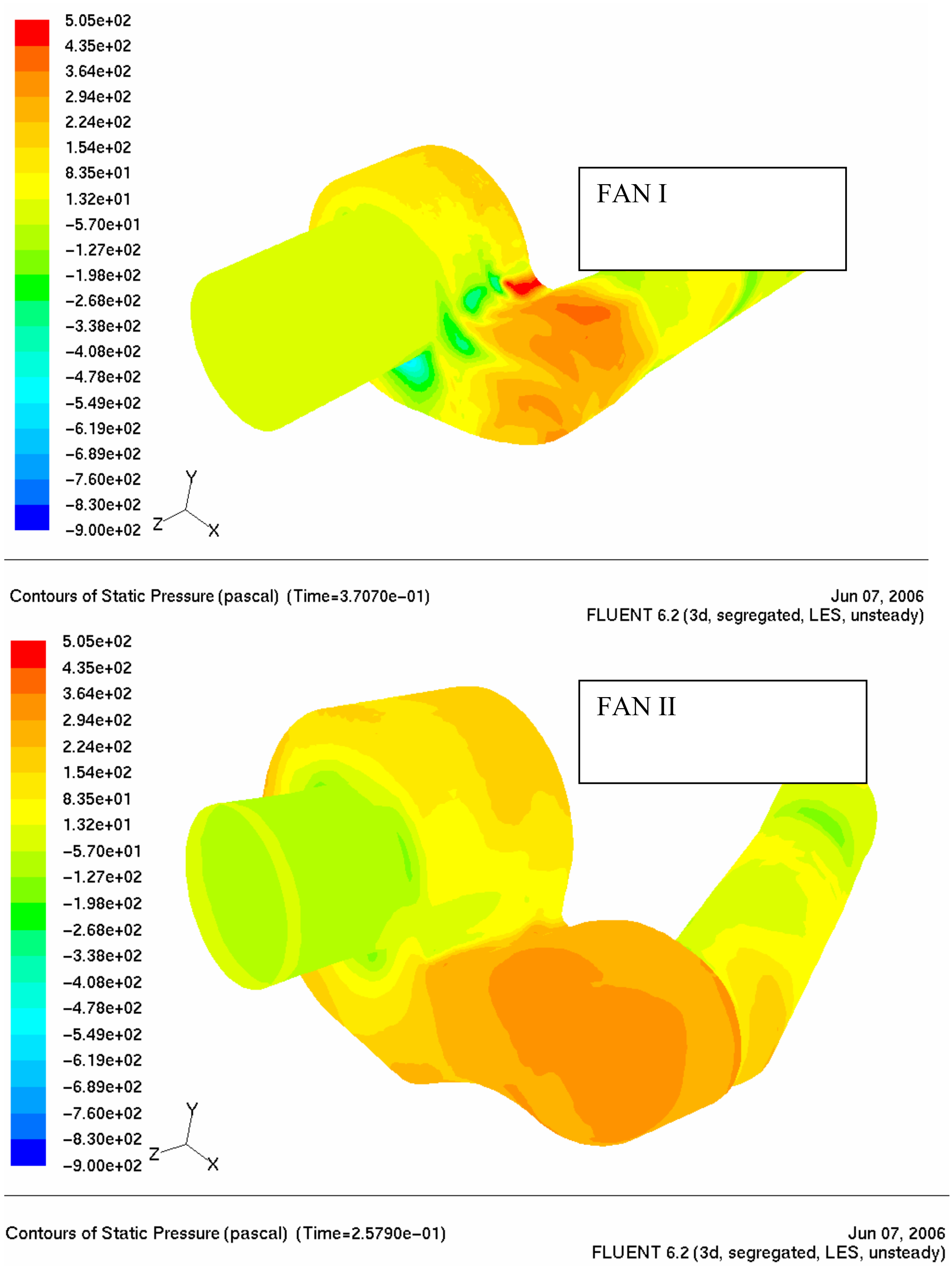

Figure 3.11: instantaneous picture of the magnitude of the pressure

Fig. 3.12 shows the instantaneous pressure distribution on the pressure and the suction side of the two designs. In the FAN I, pressure difference between suction and pressure side of the blades are given in compare to FAN II.

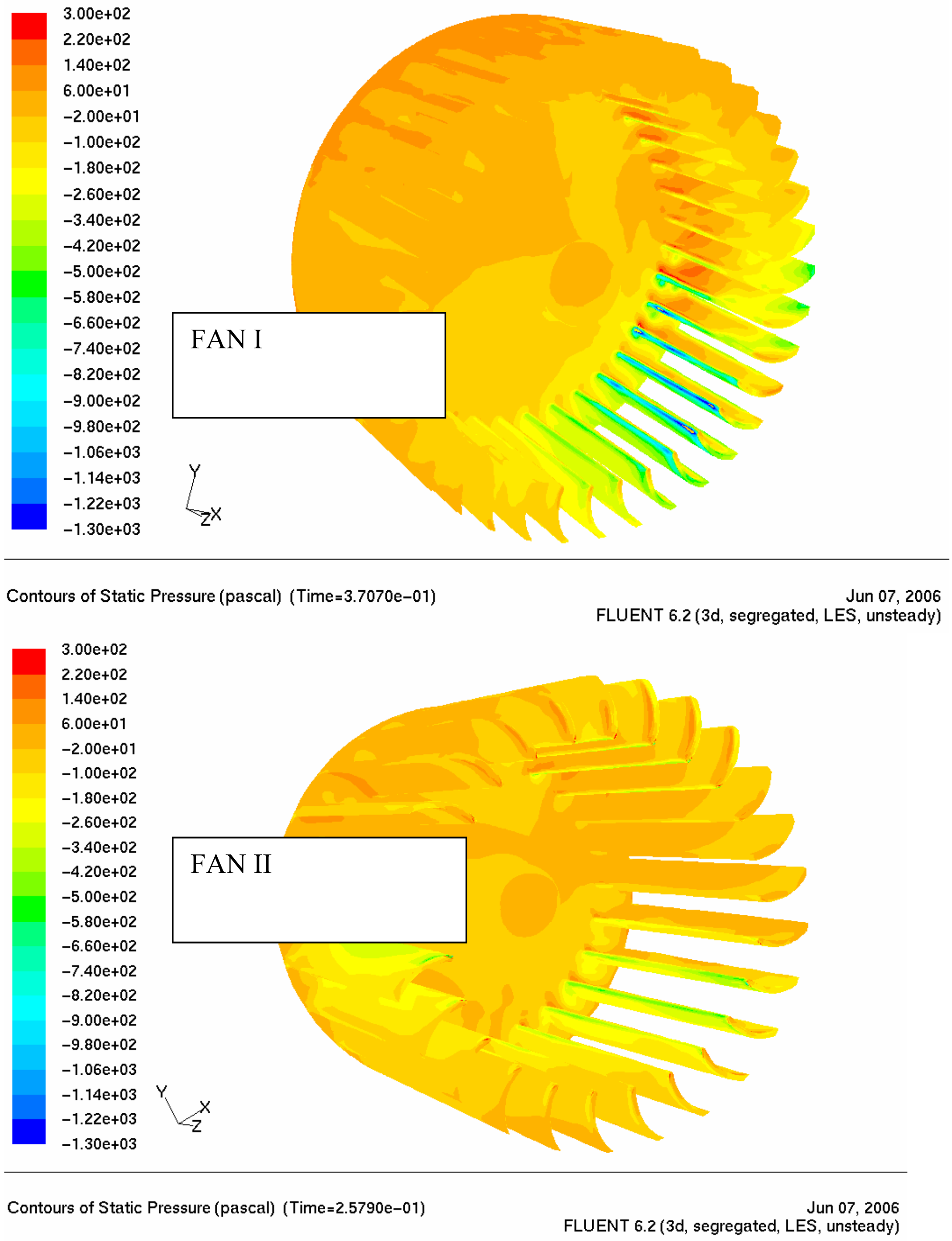

Figure 3.12: instantaneous picture of the magnitude of the pressure over fans

3.3. Computational AeroAcoustic Analysis

In this study, the commercial software SYSNOISE is employed for the AeroAcoustic analysis. SYSNOISE supports for Acoustic Boundary Element Method & Acoustic Finite Element Method computations and automatic definition of Aero-Acoustic Sources from CFD data, based on Lighthill's Aero Acoustical analogy. But, in this study, automatic definition of Aero Acoustic sources from Fluent is not used because of the problem arising "acoustically transparency". Such problems involve casing around fan have its own characteristics like acoustic modes of the cavity. In the case of automatic definition of AeroAcoustic sources from FLUENT, the solid surfaces become acoustically transparent. With the acoustically transparency problem, acoustic modes of the casing and the pipe cannot be modeled. The power of SYSNOISE is calculating Sound radiation, sound propagation and sound scattering together. But with the problem acoustically transparency, SYSNOISE can not handle the cavity acoustic modes, sound scattering from solid surfaces.

The drawback of the applying Aero Acoustic sources from FLUENT to the walls of volute in SYSNOISE, the rigid walls doesn't act as a scatter. Aero Acoustic sources create completely transparent geometry that leads to cavity acoustic modes and sound scattering effects of walls vanishes.

In this thesis, to overcome this problem a scheme is presented and a interface code written in MATLAB that permits the creation of completely nontransparent walls.. As mentioned previously, acoustic sources calculated via unsteady flow calculations. Only pressure data over one blade and over the casing exported as a function of time from FLUENT. With MATLAB code, dipole forces reconstructed from area vectors (cell area ×unit normal vector) and imported to SYSNOISE. Fig. 3.13 shows the data transfer structure of the analysis.

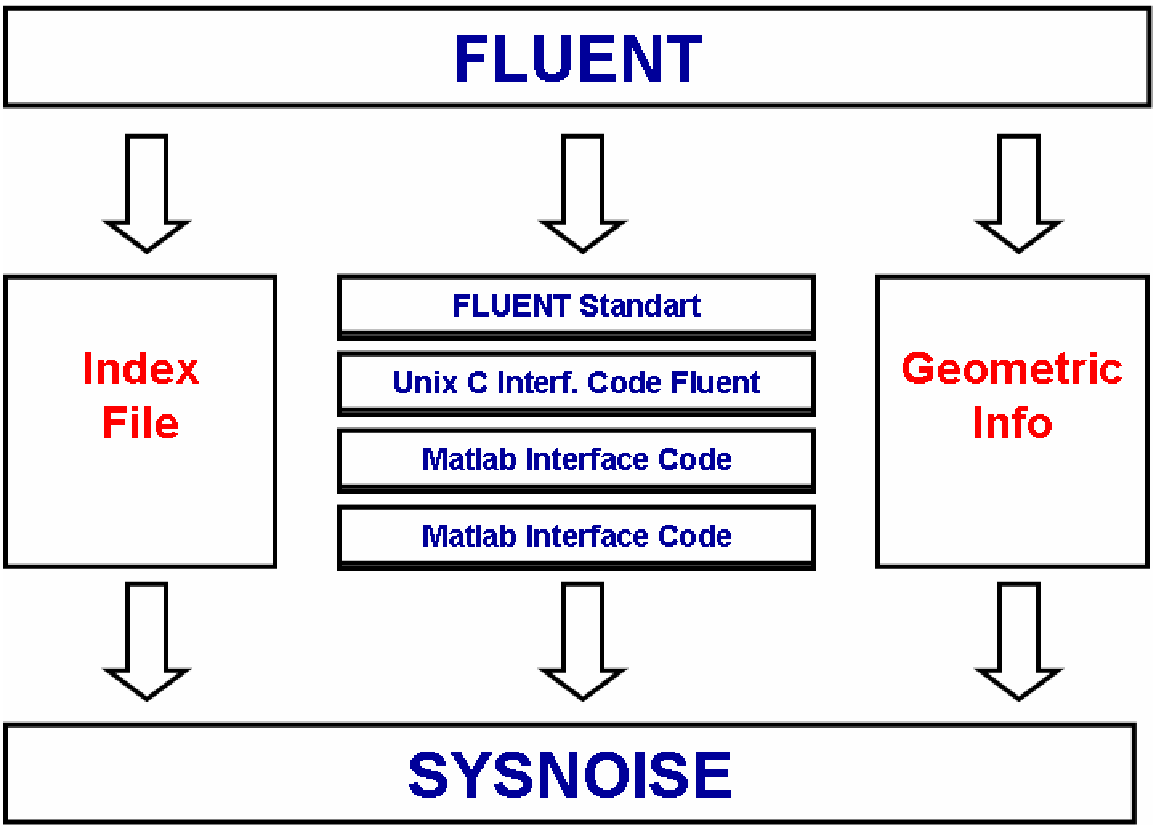

Figure 3.13: Data transfer structure

Computational grid for Aero Acoustic calculations is created with the 3D drawing/FEM solver I-DEAS. Aero Acoustic computational grid is coarse and MATLAB interface code is used for interpolation between fine CFD mesh and coarse Aero Acoustic mesh.

Aero Acoustic computation involves two steps:

1. Assigning the dipole sources over the Aero Acoustic mesh

2. Coupling between the Multi Domain BEM – Interior and Multi Domain BEM – exterior to model the acoustic modes of the cavity.

In Fig. 3.14, MDBEM Exterior and MDBEM Interior models are shown for FAN I. With assigned dipoles on Interior model, both models are coupled via openings to calculate the cavity modes of the volute and also scattering phenomenon.

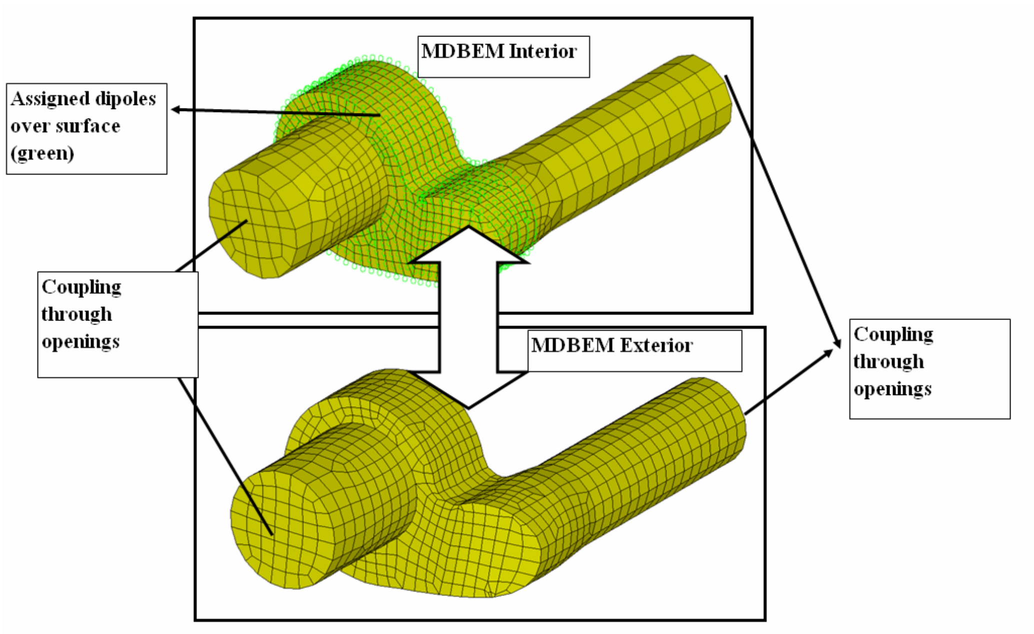

Figure 3.14: Coupling procedure for FAN I

In Fig. 3.15, the fictitious surface, both used in experiments and numerical calculations is shown. The measurement and numeric system have a reflective surface and field points to measure sound intensity.

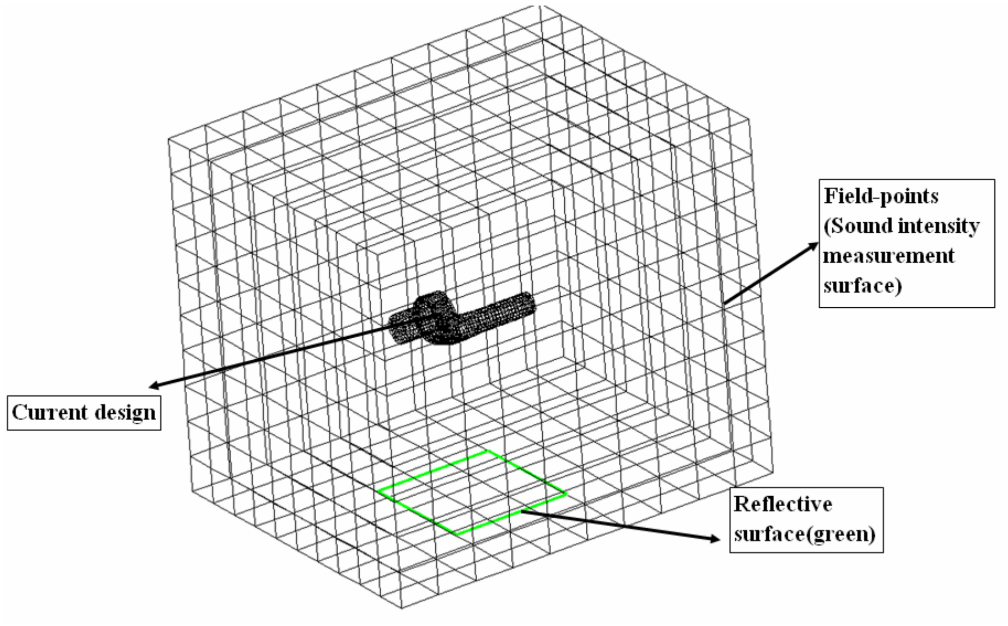

Figure 3.15: I-BEM model and sound radiation model for current design

In Fig. 3.16, MDBEM Exterior and MDBEM Interior models are shown for FAN II. With assigned dipoles on Interior model, both models are coupled via openings to calculate the cavity modes of the volute and also scattering phenomenon.

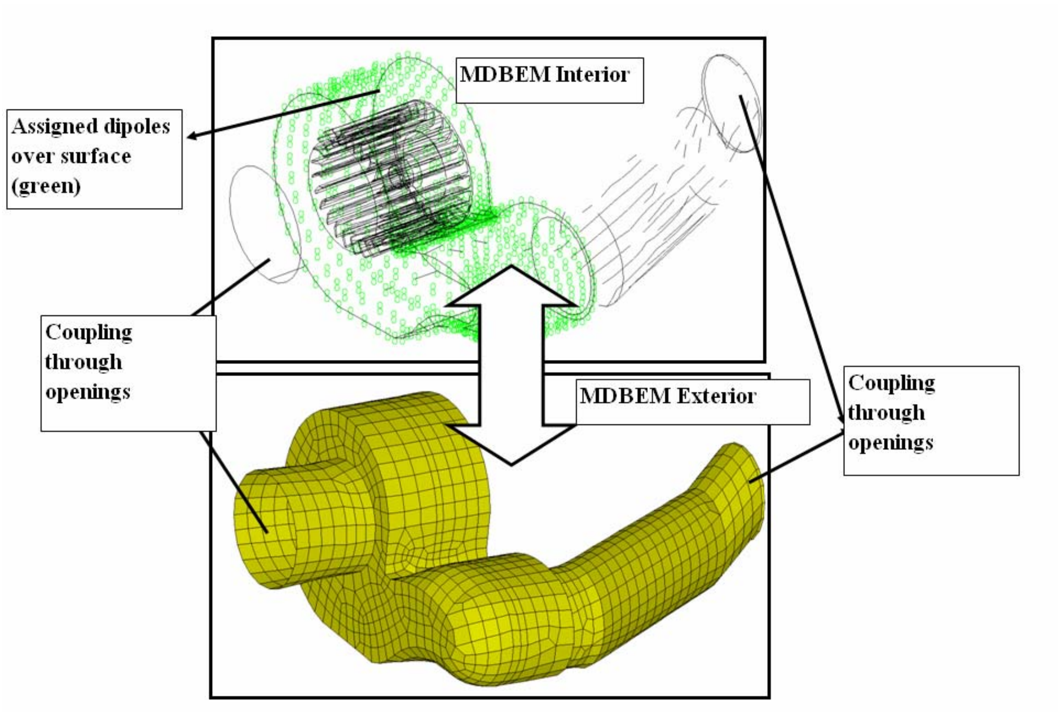

Figure 3.16: Coupling procedure for current design

In Fig. 3.17, the fictitious surface, both used in experiments and numerical calculations is shown. The measurement and numeric system have a reflective surface and field points to measure sound intensity.

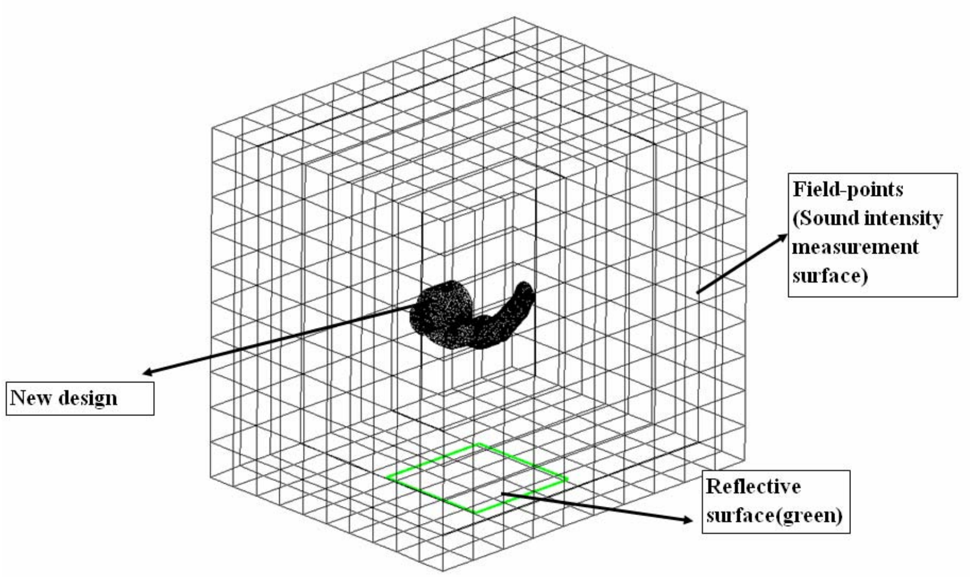

Figure 3.17: I-BEM model and soud rasiation model for current design

In this study, a distribution of surface dipole sources is created on the volute and pipe and a Multi-DBEM analysis is performed for two designs. Two models are required for this analysis, a D-BEM interior representing the inside of volute and pipe and a

D-BEM exterior representing the exterior of the volute. These two models are linked together and coupled via the pipe inlet and outlet openings. The acoustic properties for standard air is assigned in these models: speed of sound = 340 m/s and density = 1.225 kg/m^3.

3.3.1. Results

The simulations for two radial fan designs are summarized in the Figures 3.18-3.19. The acoustical results are figured according to Sound Intensity Mapping. A field point mesh is created for both designs, which define the point positions of the experiments.

270 Hz (1/12 Octave Band)

520 Hz (1/12 Octave Band)

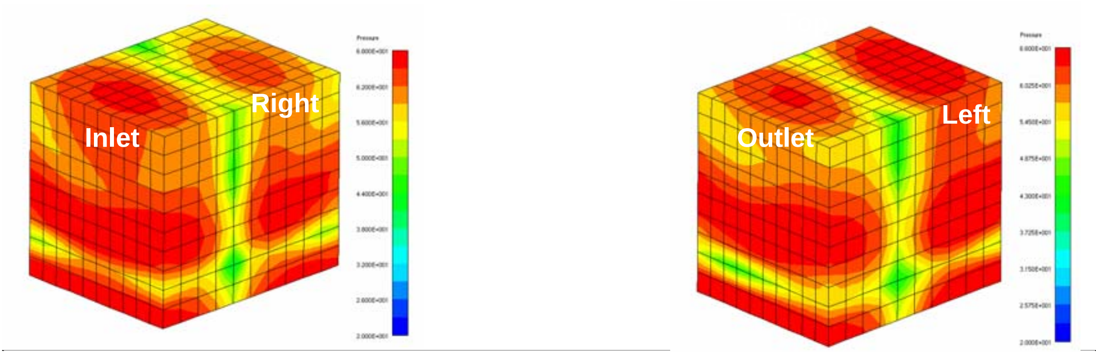

Figure 3.18: Numeric sound intensity mapping over the field point for FAN I (270 and 520 Hz (1/12 octave band))

270 Hz (1/12 Octave Band)

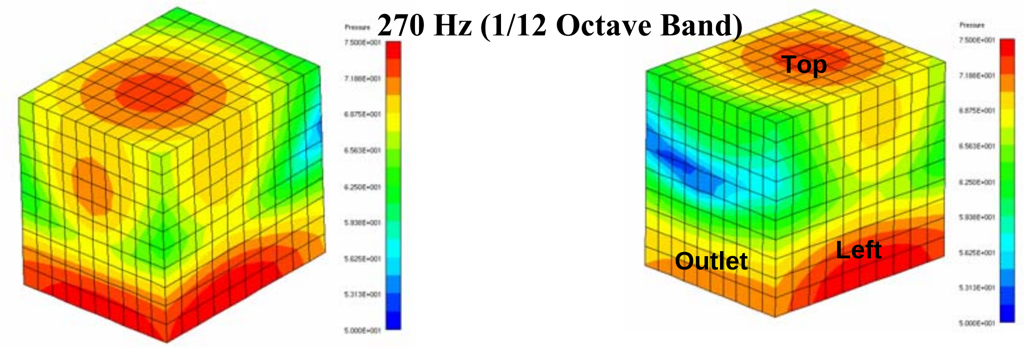

420 Hz (1/12 Octave Band)

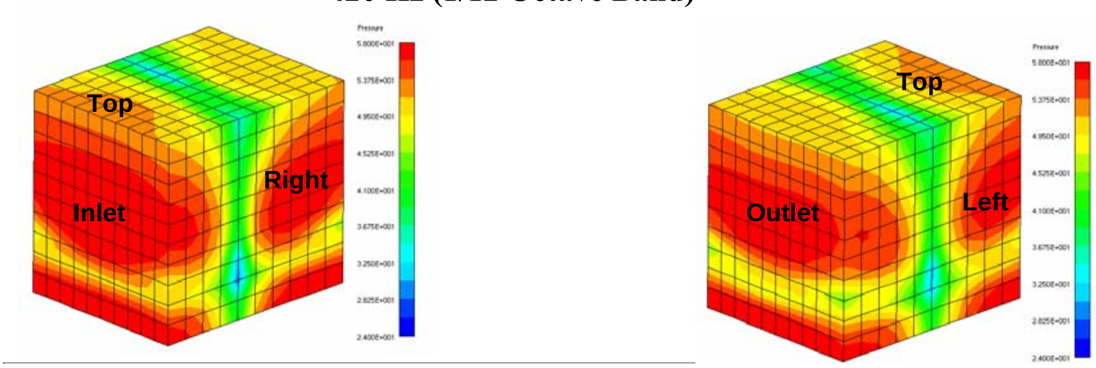

Figure 3.19: Numeric sound intensity mapping over the field point for FAN II (240 and 420 Hz (1/12 octave band))

From above figures, one can see that the FAN II has a lower sound power level in comparison to FAN I. With same color scale range, the directivity show different characteristics from one cavity frequency to another. However, sound pressure levels are different, but directivity pattern are very similar for two designs.

4. EXPERIMENTS

Sound intensity measurements are done for both designs over a rectangular box in which fans are located. Sound intensity is the time-averaged product of the pressure and particle velocity. It is possible to measure pressure gradient with two closely spaced microphones and relate it to particle velocity.

The use of sound intensity rather than sound pressure to determine the sound power means that the measurement can be made in situ, with steady background noise and in the near field of machines. The sound power is the average normal intensity over a surface enclosing the source, in our case fan-volute system, multiplied by the surface area. The fictitious surface is shown in Fig. 4.1.

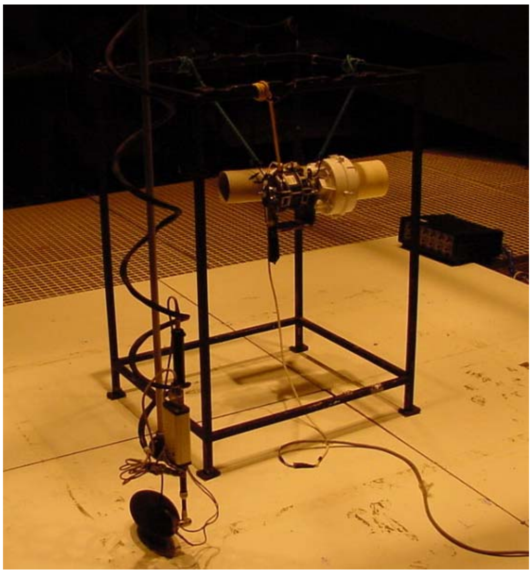

FAN I

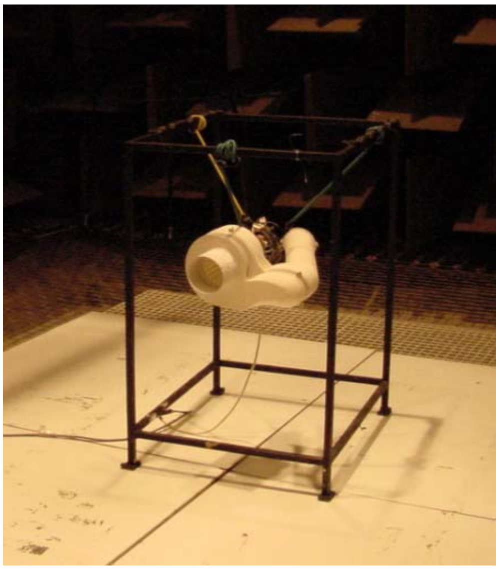

FAN II

Figure 4.1: Experimental set-up for both sound intensity and sound pressure measurements

Any enclosing surface can be chosen as long as no other sources or absorbers of sound are present within the surface. The floor is assumed to reflect all the power hence so need not be included in the measuring surface. The surface may, in theory, be any distance from the acoustic source.

5. COMPARISON OF NUMERICAL AND EXPERIMENTAL RESULTS

The experimental SPL curve is smoother than the numerical curve. In the experiments, the acoustic signal is measured for about 10 s. However, in the simulation the total time for the acoustic evaluation is about 0.125 s, which corresponds to about 5 rotations of the propeller. In the experiments the acoustic signal of about 500 rotations is evaluated. Since the frequency analysis is performed with far less data in the simulation than it is available in the experiment, the numerical SPL curve has more fluctuations than the experimental curve. If the acoustic computation is carried out for longer time, these fluctuations will disappear; but the general shape of the curve will remain the same.

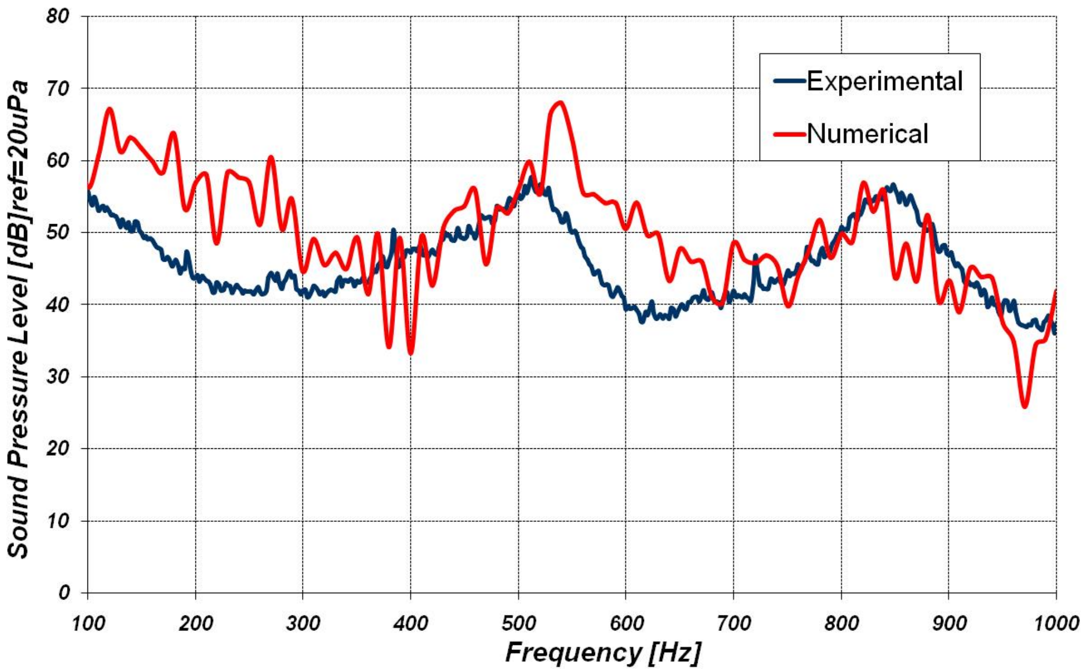

Figure 5.1: Sound pressure level spectrum from computations and exoeriments of FAN II

As can be seen in Fig.5.1, the numerical prediction of the acoustic signal in the far field matched the experimental measurements satisfactorily for FAN II.

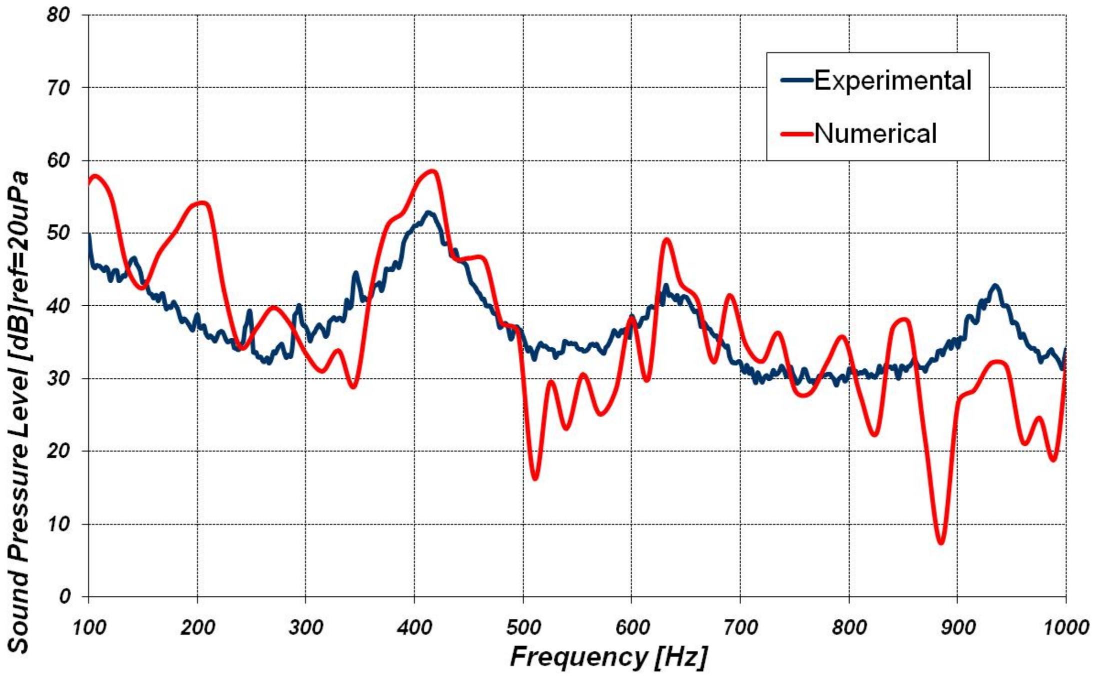

Figure 5.2: Sound pressure level spectrum from computations and experiments of FAN I

It is also seen in Fig.5.2. that the acoustic prediction agrees with the experimental measurements in the case of FAN I.

From Figures 5.3-5.6, one can see that the for both FAN I and FAN II, the CAA-tool is tested with high accuracy. The first test case is the prediction of the flow noise of a radial fan currently used in laundry dryers with high Sound Power Level. Simulations of the flow in the flow domain of fan-volute system show that LES is a reliable flow simulation method. The aerodynamical characteristics of the flow are predicted with high accuracy. Consequently, the acoustic prediction and directivity of the sound agrees with the experimental measurements.

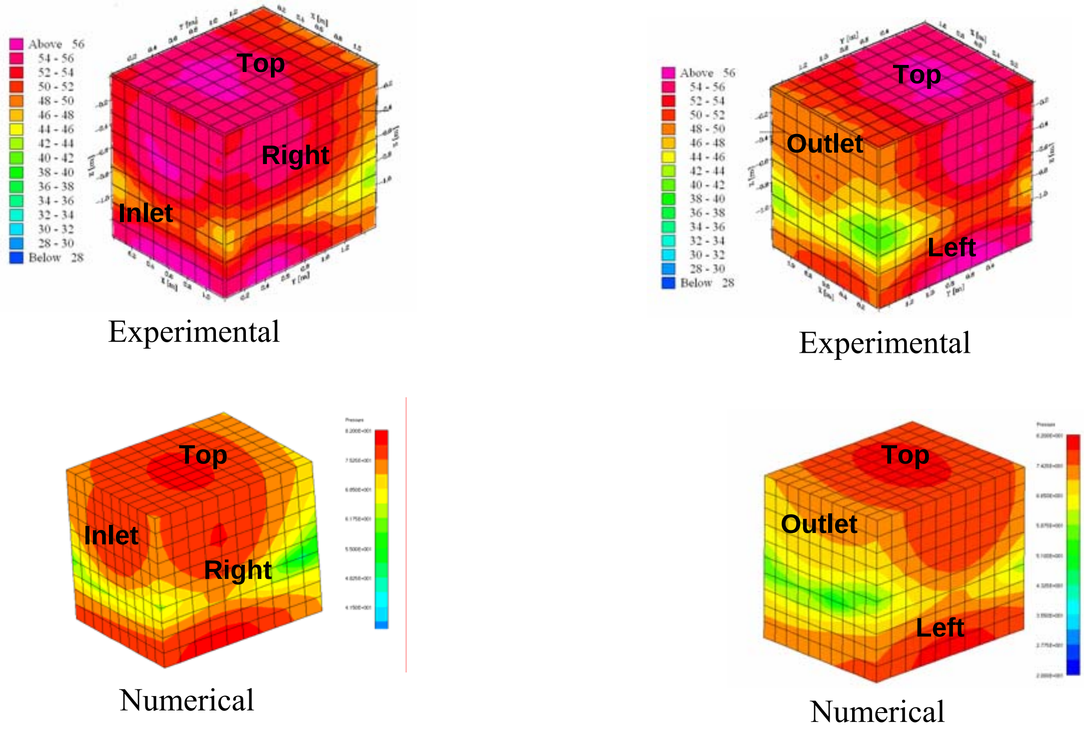

Figure 5.3: Numeric and experimental sound intensity mapping over the field point for FAN I (270Hz (1/12 octave band))

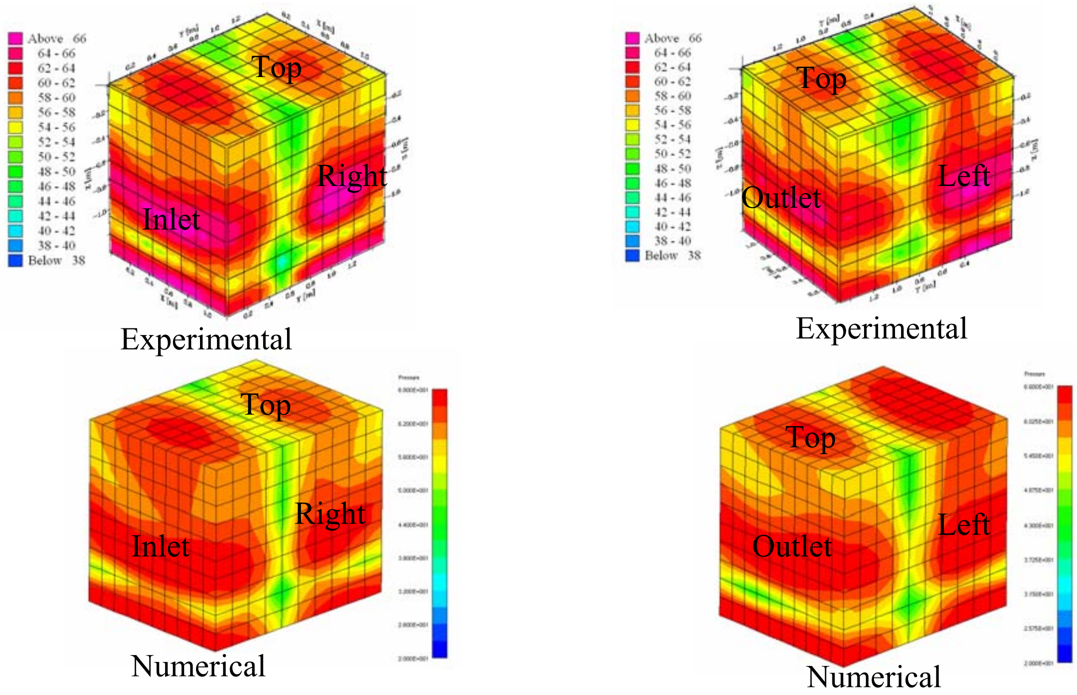

Figure 5.4: Numeric and experimental sound intensity mapping over the field point for FAN I (520 Hz (1/12 octave band))

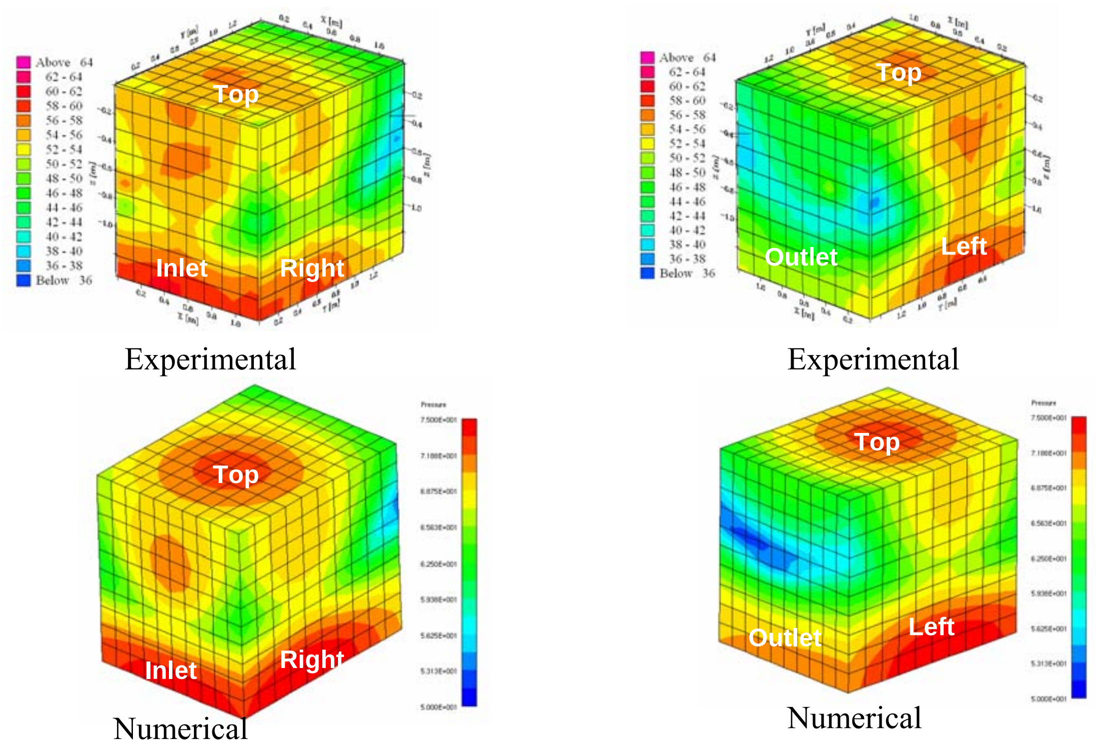

Figure 5.5: Numeric and experimental sound intensity mapping over the field point for FAN II (240 Hz (1/12 octave band))

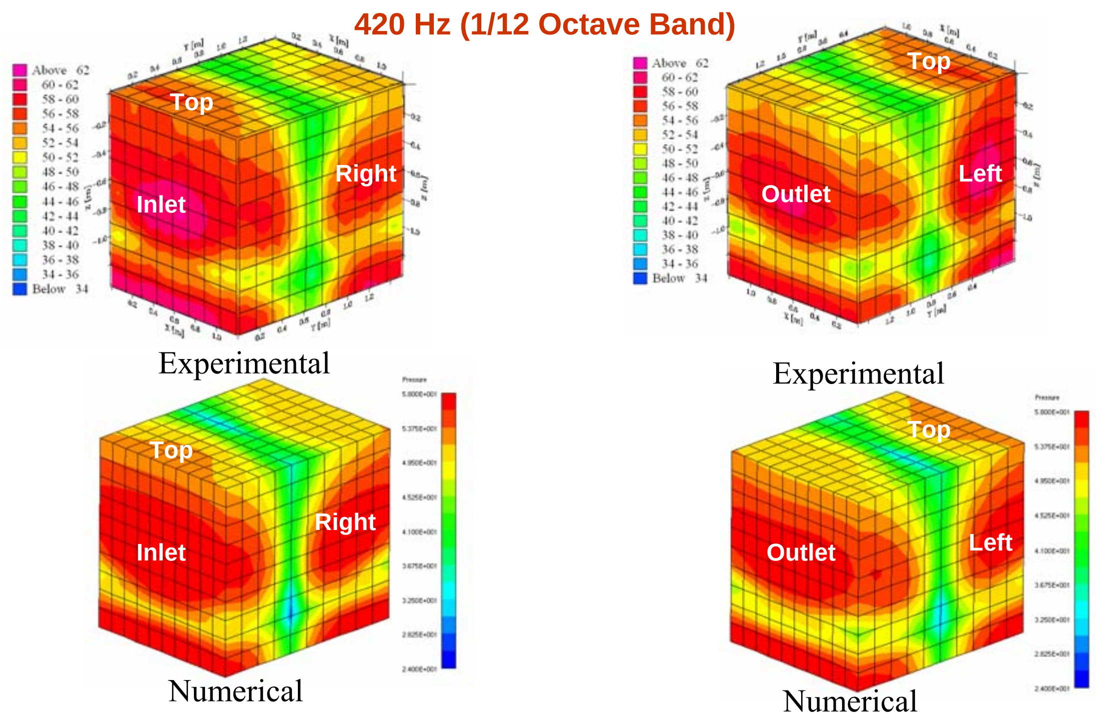

Figure 5.6: Numeric and experimental sound intensity mapping over the field point for FAN II (420 Hz (1/12 octave band))

And finally, the CAA-tool calculated the total sound power level with high accuracy. In Figure 5.7, the comparison of the sound power levels measured and predicted for FAN I is given. In computations the sound power level of FAN I is predicted ~1.5 dBA lower than the experiments

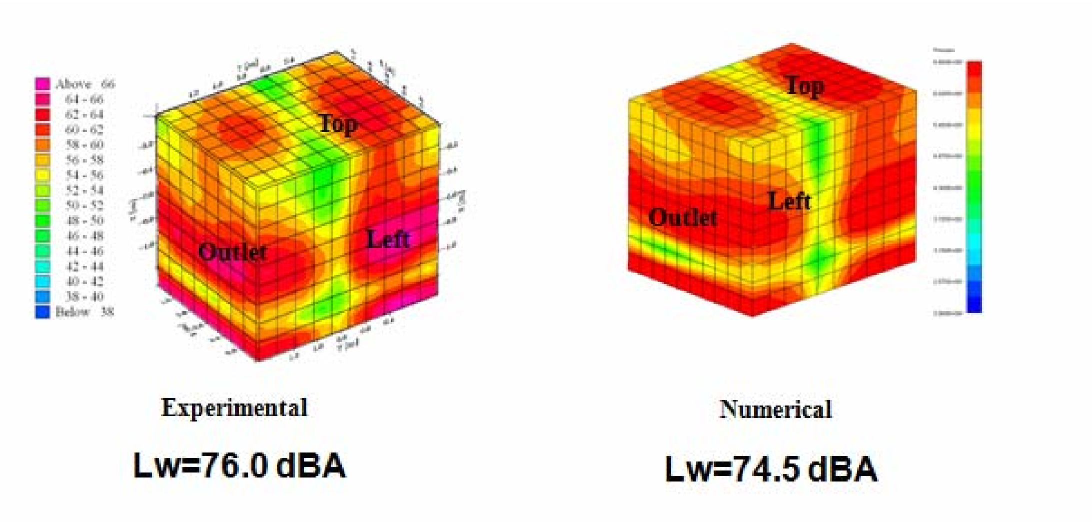

Figure 5.7: Numeric and experimental sound power level comparision for FAN I

In Figure 5.8, the comparison of the sound power levels measured and predicted for FAN II is given. In computations the sound power level of FAN II is predicted ~2 dBA higher than the experiments.

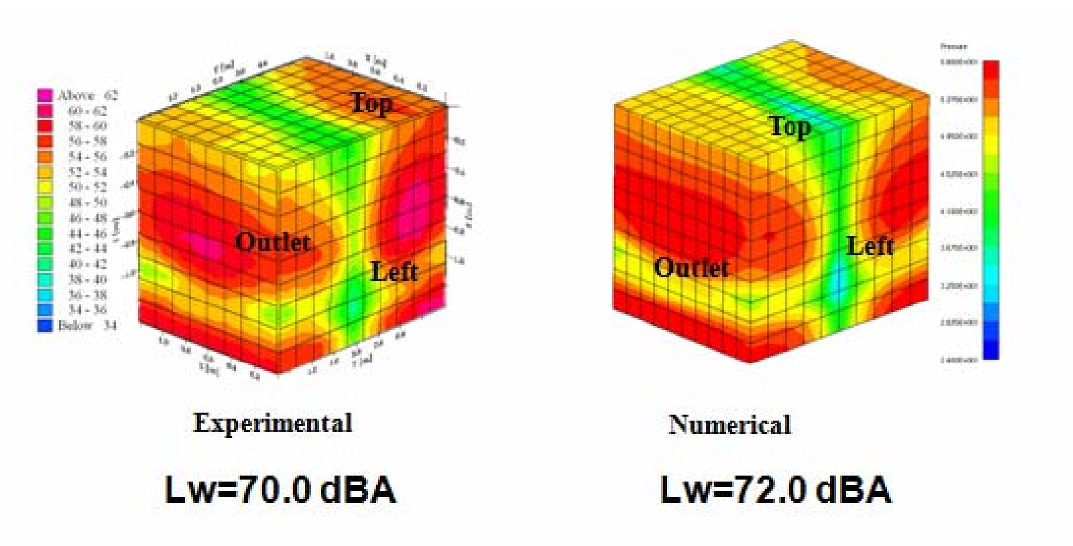

Figure 5.8: Numeric and experimental sound power level comparision for FAN II

6. CONCLUSION AND OUTLOOK

In the frame of this work, a reliable and accurate CAA-tool is presented, which is developed for the purpose of the far field noise prediction for radial fans. The CAA-tool performs time accurate CFD simulation in the first step with the help of commercial software FLUENT and then computes the far field acoustic signal based on the computed unsteady flow data with the Ffowcs Williams and Hawkings acoustic analogy using commercial AeroAcoustic software SYSNOISE.

The CAA-tool is tested with two validation cases. The first test case is the prediction of the flow noise of a radial fan currently used in laundry dryers with high Sound Power Level. Simulations of the flow in the flow domain of fan-volute system show that LES is a reliable flow simulation method. The aerodynamical characteristics of the flow are predicted with high accuracy. Consequently, the acoustic prediction agrees with the experimental measurements.

A drawback of LES is that it requires more computational power and CPU-time than uRANS. Nevertheless, in computational acoustics where the accuracy is especially important, the additional requirements are worth the cost. In order to assure the accuracy in LES, the spatial resolution of the computational grid has to be fine enough.

Second test case is the flow in another radial fan-volute system that designed to replace the first system and has a lower Sound Power Level. This configuration is an enhancement of the first test case. Because of the lack of the aerodynamical measurements, only acoustic data is compared with the experiment. The numerical prediction of the acoustic signal in the far field matched the experimental measurements satisfactorily.

The presented CAA tool is proven to be a valuable tool for the far field noise prediction. The additional computational memory and CPU-time requirements are relatively low. The acoustic software SYSNOISE is robust, fast and easy to handle. The accuracy of the acoustic prediction depends solely on the accuracy of the CFD data. Since the CAA-tool is satisfactorily validated, the tool can be employed in the near future for designing low noise fan systems.

7. REFERENCES

[1] Lighthill, M. J.,1952, On Sound Generated Aerodynamically: I. General Theory, *Proceedings of the Royal Society of London,* Series A, Vol. 211, pp. 564-587.

[2] Lighthill, M. J., 1978, On Sound Generated Aerodynamically: II. Turbulence as a Source of Sound, *Proceedings of the Royal Society of London*, Series A, Vol. 222, pp. 1-32, 1954.

[3] Lighthill, M. J., 1978 Waves in Fluids, *Cambridge University Press*, ISBN 0-521-29233-6,.

[4] Curle, N., 1955, The Inuence of Solid Boundaries upon Aerodynamic Sound, *Proceedings of the Royal Society of London*, Series A, Vol. 231, pp. 506-514,.

[5] Ffowcs Williams, J. E., Hawkings, D., L., 1969, Sound Generation by Turbulence and Surfaces in Arbitrary Motion, *Philosophical Transactions of the Royal Society of London*, Vol. 264, No. A 1151, pp. 321-342, .

[6] Page, G. J., McGuirk, J. J., Hossain, M., Self, R., Bassetti, A., 2003, A CFD coupled acoustic approach for coaxial jet noise, *AIAA paper, AIAA* 2003-3286,.

[7] Bailly, C., Candel, S., Lafon, P., 1996, Prediction of Supersonic Jet Noise from a Statistical Acoustic Model and a Compressible Turbulence Closure, *Journal of Sound and Vibration 194(2),* pp. 219-242,.

[8] Bogey, C., Bailly, C., 2002, Downstream sunsonic jet noise: link with vortical structures intruding into the jet core, *C. R. Mecanique 330,* pp. 527-533,.

[9] Ewert, R., Schröder, W., 2004, On the simulation of trailing edge noise with a hybrid LES/APE method, *Journal of Sound and Vibration 270,* pp. 219-242,.

[10] Sorgüven, E., 2004. A Computational Aeroacoustics Method Using Large eddy Simulation and Acoustic Analogy, *Phd Thesis,* University of Karlsruhe, Germany.

[11] Bommes, L., Fricke, J., Klaes, K., 2003, Ventilatoren, Vulkan Verlag, Essen,.

[12] Carolus, T., 2003, Ventilatoren – Aerodynamischer Entwurf, Schallvorhersage, Konstruktion, Teubner Verlag, Wiesbaden,

[13] Velarde, S., Rafael, B., 2005, A predictive maintenance procedure using pressure and acceleration signals from a centrifugal fan , *Applied Acoustics 67,* pp. 219-242,.

[14] Marretta, R.M.A., Tassone, G., 2001, A vorticity based aeroacoustic prediction for the noise emission of a low-speed turbulent internal flow , *Computers & Fluids 32,* pp. 457-478,.

[15] Ianniello, S., 2001, Aeroacoustic analysis of high tip-speed rotating blades, *Aerosp. Sci. Technol. 5,* pp. 179-192,.

[16] Lin, S.C., Huang, C.L., 2001, An integrated experimental and numerical study of forward-curved centrifugal fan , *Experimental Thermal and Fluid Science 26,* pp. 421-434,.

[17] Jeon, W.H., Baek, S.J., Kim, C.J., 2002, Analysis of the aeroacoustic characteristics of the centrifugal fan in a vacuum cleaner, *Journal of Sound and Vibration 268,* pp. 1025-1035,.

[18] Suh, J., Frankel, S.H., Mongeau, L., Plesniak, M.W., 2006, Compressible large eddy simulations of wall-bounded turbulent flows using a semi-implicit numerical scheme for low Mach number aeroacoustics, *Journal of Computational Physics 215,* pp. 526-551,.

[19] Bogey, C., Bailly, C., 2004, Computation of a high Reynolds number jet and its radiated noise using larhe eddy simulation based on explicit filtering, *Computers & Fluids 32,* pp. 525-535,.

[20] Ryu, J., Cheong, C., Sungtae, K., Soogab, L., 2005, Computation of internal aerodynamic noise from a quick-opening throttle valve using frequency-domain acoustic analogy, *Applied Acoustics 66,* pp. 1278-1308,.

[21] Nallasamy, M., Envia, E., 2005, Computation of rotor wake turbulence noise, *Journal of Sound and Vibration 282,* pp. 649-678,.

[22] Kim, H. H., Lee, S., Fujisawa, N., 2006, Computation of unsteady flow and aerodynamic noise of NACA0018 airfoil using large-eddy simulation, *International Journal of Heat and Fluid Flow 27,* pp. 229-242,.

[23] Gerard, A., Berry, A., 2005, Control of tonal noise from subsonic axial fan. Part 1: reconstruction of aeroacoustic sources from far-field sound pressure, *Journal of Sound and Vibration 288,* pp. 1049-1075,.

[24] Maaloum, A., Kouidri, S., Bakir, F., Rey, R., 2003, Effect of inlet duct contour and lack thereof on the noise generated of an axial fan, *Applied Acoustics 64,* pp. 999-1010,.

[25] Velarde, S., Tajadura, R., 2006, Experimental determination of the tonal noise sources in a centirfugal fan, *Journal of Sound and Vibration 295,* pp. 781-796,.

[26] Polacsek, C., Desbois, F., 2003, Fan interaction noise reduction using a wake generator: experiments and computational aeroacoustics, *Journal of Sound and Vibration 265,* pp. 725-743,.

[27] Özyörük, Y., Alpman, E., 2004, Frequency-domain prediciton of turbofan noise radiation, *Journal of Sound and Vibration 270,* pp. 933-950,.

[28] Wu, S.F., Su, S., 1997, Modelling of the noise spectra of axial flow fans in a free field, *Journal of Sound and Vibration 200,* pp. 379-399,.

[29] Wu, S.F., Su, S., 1998, Noise radiation from engine cooling fans, *Journal of Sound and Vibration 216,* pp. 107-132,.

[30] Kato, C., Yamade, Y., 2007, Numerical prediction of sound generated from flows with a low Mach number, *Computers & Fluids 36,* pp. 53-68,.

[31] Velarde, S., Tajadura, R., 2006, Numerical simulation of the aerodynamic tonal noise generation in a backward-curved blades centrifugal fan, *Journal of Sound and Vibration 295,* pp. 781-796,.

[32] Lee, S., Kim, J., 1997, Prediction of rotor high-speed impulsive noise with a combined CFD-Kirchhoff method, *Journal of Sound and Vibration 207,* pp. 453-464,.

[33] Mihaescu, M., 2005, Computational aeroacoustics based on large eddy simulations and acoustic analogies, *Phd Thesis,* Lund Institute of Technology, Sweden.

[34] Munz, C., Fortenbach, R., 2005, Multiple-scale modelling of acoustic soyrces in low Mach-number flow, *C.R. Mecaniwue 333,* pp. 706-712,.

[35] Gloerfelt, X., Lafon, P., 2005, Direct computation of the noise induced by a turbulent flow through a diaphram in a duct at low Mach number, *Euromech Colloquium 467: Turbulent Flow and Noise Generation*

[36] Wilcox, D.C., 2002, Turbulence Modeling for Cfd, D C W Industries

[37] Liu, S., Meneveau, C., 1994, On the properties of similarity subgrid-scale models as deduced from measurements in a turbulent, *Journal of Fluid Mechanics 275,* pp. 83-119,.

[38] Goldstein, M.E., 1976, Aeroacoustics, McGraw-Hill Book Company, New York 275, pp. 83-119,.

[39] Rayleigh, J.W.S., 1929, The Theory of Sound, 2ndedition, MacMillan and Co. Ltd., London,.

[40] Bretner, K.S., 1997, An efficient and robust method for predicting helicopter high-speed impulsive noise, *Journal of Sound And Vibration 203,* pp. 87-104,.

[41] Ianniello, S., 1999, Algorith to integrate the Ffowcs Williams-Hawking Equation on Supersonic rotating domain, *AIAA Journal, 37*, pp. 1040-1047,.

[42] Farassat, F., Brentner, K.S., 1998, Supersonic quadrupole noise theory for high-speed helicopter rotors, *Journal of Sound And Vibration 218*, pp. 418-500,.

[43] Farassat, F., Brentner, K.S., 1987, The uses and abuses of the acoustic analogy in helicopter rotor noise prediction, *NASA Langley Technical Report Server*,.

[44] Slimon, S.A., 1999, Computational aeroacoustics simulations using the expansion about incompressible flow approach, *AIAA Journal, 37*, pp. 409-416,.

[45] Boudet, J., Casalino, M.C., 2004, Prediction of broadband noise: airfoil in the wake of a rod, *42nd AIAA Aerospace Sciences Meeting and Exhibit, paper AIAA-2004-0852, Reno (NV, USA)*,.

8. CIRRUCULUM VITAE

Yılmaz DOĞAN was born in SIVAS in 1983. He graduated from Istanbul Technical University, Mechanical Engineering Faculty with Bachelor of Science, Mechanical Engineer in 2004. Same year, he started his Master of Science education at İTÜ, Machine Dynamic, Vibration and Acoustics program. He is working as an R&D engineer at Arçelik A.Ş. and studying his master thesis.